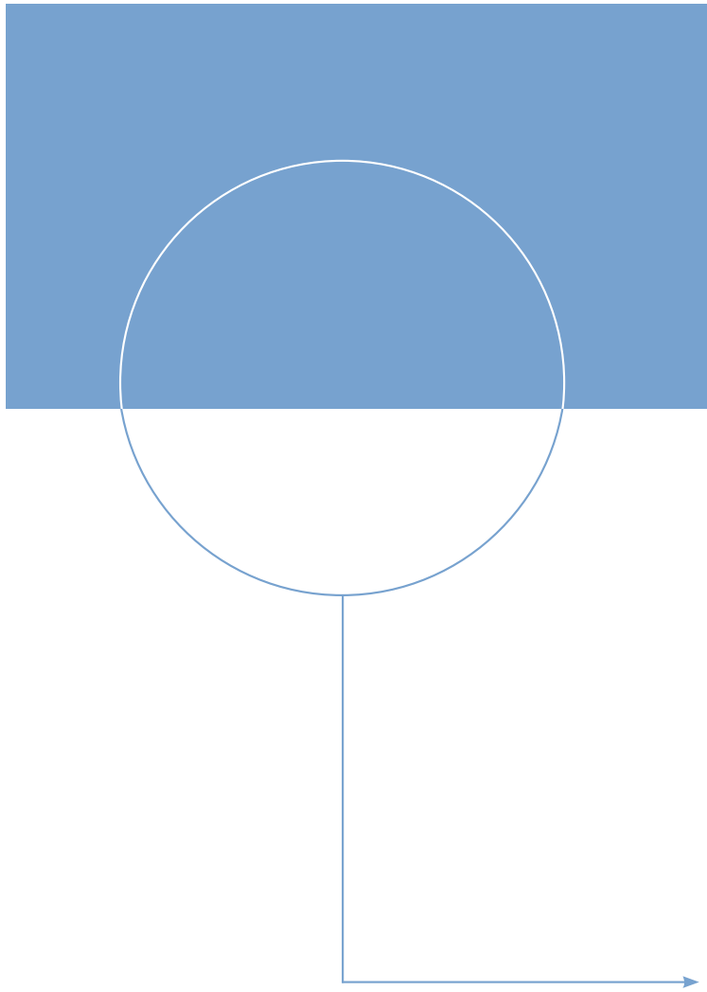

Master's thesis

2019

Lene Jensberg Hansen

NTNU
Norwegian University of
Science and Technology
Faculty of Natural Sciences
Department of Materials Science and Engineering

Lene Jensberg Hansen

Rheological Characterization of Fluid Models for Pitch and Binder Matrix in Anodes

June 2019

NTNU
Norwegian University of
Science and Technology

NTNU
Norwegian University of
Science and Technology

NTNU

Norwegian University of
Science and Technology

Rheological Characterization of Fluid Models for Pitch and Binder Matrix in Anodes

Lene Jensberg Hansen

Materials Science and Engineering
Submission date: June 2019
Supervisor: Tor Grande IMA
Co-supervisor: Houshang Alamdari, Université Laval
Roozbeh Mollaabbasi, Université Laval

Norwegian University of Science and Technology
Department of Materials Science and Engineering

Preface

This master's thesis is written as a part of the Master Program Materials Science and Engineering at the Norwegian University of Science and Technology (NTNU) during the spring of 2019. The work presented in this thesis was carried out as a research internship at the Department of Mineral, Metallurgical and Materials Engineering at Université Laval, Québec, Canada under the International Partnerships for Excellent Education and Research by the Norwegian Research Council (IntPart) project: Norwegian-Canadian Partnership in Research and Education on Primary Production of Aluminium (CaNAl). The thesis is part of a larger on-going project at Université Laval with the Aluminium Research Centre RÉGAL on the detailed understanding of the physics of anode compaction that will continue after the completion of this degree. Financial support was received from the Research Council of Norway through the CaNAl project and from Université Laval. Professor Tor Grande (NTNU) has been my supervisor and professor Houshang Alamdari (Université Laval), and postdoctoral fellow Roozbeh Mollaabbasi (Université Laval) have been my co-supervisors.

I would like to extend my thanks to Tor Grande for introducing me to the anode production process, and for guidance and support throughout the year. I am also grateful for the opportunity to go to Canada and Université Laval as a part of the CaNAl project. Houshang Alamdari deserves my gratitude for his hospitality and support before and during my stay. I want to thank Roozbeh Mollaabbasi for introducing me to the project and rheology, and for always being available for support, guidance, directions and help. The technical support and help from the rest of the staff at Université Laval are greatly appreciated. A huge thanks to Mounir Baiteche for his hospitality

and for showing us Québec. Lastly, I would thank Trond Brandvik for his continuous support despite being relieved of his supervising duties and a great time in Québec.

Trondheim, June 23rd 2019

Lene Jensberg Hansen

Abstract

Carbon anodes are used to produce primary aluminium and are consumed in the electrolysis. Anodes must consequently be continuously replaced and produced. Major issues encountered in anode processing include heterogeneous density and cracks that may cause preferential current paths, uneven anode consumption and breakage. It is therefore of great interest to improve understanding of the anode production process. Green anodes are made of a paste containing coarse coke particles, surrounded by a binder matrix consisting of fine coke particles and coal-tar pitch binder. Binder matrix is a viscoelastic material that deforms around the coarse coke particles and enters into their pores. The rheological properties of pitch and binder matrix are important parameters influencing the final anode quality. Investigating the green anode paste behavior during forming and compaction can reveal the interaction between binder matrix and coarse coke particles. Due to high processing temperatures introducing complications such as temperature gradients and temperature variations, experimenting on pitch and binder matrix is challenging. Fluid models with potential similar rheological properties as pitch and binder matrix have been tested at room temperature. A rheometer was used for rotational and oscillation testing. Optical transparency of fluid models has been evaluated for visualization of the movement of coarse coke particles during compaction, as the lack of optical contrast between binder matrix and coarse coke particles prevent visualization. Existing data on rheological properties of pitch and binder matrix have been compared to suspension models, and the effect of properties in addition to fine coke particle volume fraction on viscosity have been addressed.

Sammendrag

Karbonanoder brukes til å produsere primæraluminium og forbrukes i løpet av elektrolysen. Anodene må derfor kontinuerlig erstattes og produseres. Problemer relatert til prosesseringen av anoder inkluderer heterogen tetthet og sprekker som kan føre til at strømmen går i andre baner i elektrolysen, anoden forbrukes ujevnt og brudd kan forekomme. Forbedret forståelse av anodeproduksjonsprosessen er således av stor interesse. Grønnanoder er laget av en masse som inneholder grove kokspartikler, som omringes av "binder matrix", bestående av fine kokspartikler og kulltjærebek bindemiddel. "Binder matrix" er et viskoelastisk materiale som deformeres rundt de grove kokspartiklene og går inn i porene deres. De reologiske egenskapene til bek og "binder matrix" er viktige parametere som påvirker den endelige anodekvaliteten. Samspillet mellom "binder matrix" og grove kokspartikler kan avdekkes ved å undersøke hvordan grønnanodemassen oppfører seg under forming og komprimering. Høye prosesstemperaturer introduserer komplikasjoner som temperaturgradienter og temperaturvariasjoner slik at forsøk på bek og "binder matrix" er utfordrende. Modellfluider som potensielt har lignende reologiske egenskaper som bek og "binder matrix" har blitt testet i romtemperatur. Et reometer ble brukt til roterende og oscillerende tester. Modellfluidenes optiske gjennomsiktighet ble vurdert for visualisering av de grove kokspartiklenes bevegelse under komprimering, da det ikke er noen optisk kontrast mellom "binder matrix" og grove kokspartikler som muliggjør visualisering. Eksisterende data på de reologiske egenskapene til bek og "binder matrix" har blitt sammenlignet med suspensjonsmodeller, og effekten av egenskaper i tillegg til volumfraksjon av fine kokspartikler på viskositet har blitt adressert.

Contents

Chapter 1

Introduction

1.1 Background

The total amount of primary aluminium produced in 2018 was more than 64 million tonnes [1]. This is an increase of approximately 60 % since 2008, and the prognosis indicates that the production will continue to increase. The Hall-Héroult electrolysis process is the major process for the production of primary aluminium metal [2]. In this process, alumina (Al_2O_3) is dissolved in molten electrolyte and is reduced to molten aluminium at the cathode. The oxygen reacts with the carbon anode to carbon oxides. The overall reaction for the process is:

$$2Al_2O_3(\text{dissolved}) + 3C(s) = 4Al(l) + 3CO_2(g) \tag{1.1}$$

As the carbon anodes are consumed during the electrolysis, they must be continuously replaced. The most common anodes used today are prebaked anodes, which are formed and calcined before being installed in the electrolysis cell [3]. A flowchart of the production of prebaked anodes is presented in Figure 1.1. The main components of green anodes are calcined petroleum coke (CPC), recycled anode butts and coal-tar pitch as binder [4]. After the components have been blended and mixed, the resulting anode paste enters a vibro-compactor or a hydraulic press to be formed and den-

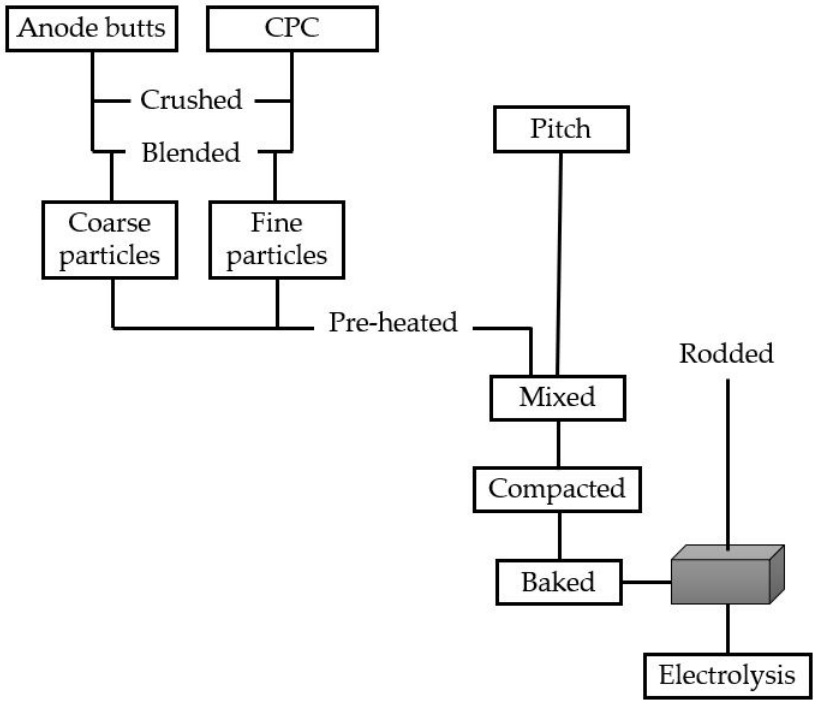

Figure 1.1: Flow chart of production of prebaked anodes.

sified at elevated temperatures [4]. The last step of the anode production process is baking the anode in a furnace up to approximately 1200 °C for ~14-17 days [5]. Coal-tar pitch is carbonized during baking, and the anodes become mechanically strong, ready to be used in the electrolysis.

The final quality of the anodes strongly depends on the physical and chemical properties of the anode paste [6]. The main goals in anode production include having high and homogeneous anode density while also avoiding cracks. Density gradients in the anode may cause preferential current paths, non-uniform anode consumption, and possible breakage during baking or in the electrolysis.

There are generally two size ranges of coke particles used in the anode paste: coarse particles (> 0.15 mm and < 9.5 mm) and fine particles (< 0.15 mm) [7]. The fine particles and coal-tar pitch binder are defined as the binder matrix of the anode paste, surrounding the coarse particles. Coal-tar pitch is solid at room temperature and behaves as a Newtonian fluid at compaction temperature of approximately 178 °C [8]. During compaction, the binder matrix is a viscoelastic material that deforms and moves

around and into the pores of coarse particles [9]. The rheological properties of the binder matrix are therefore important for the understanding of the compaction behavior of anode paste. Factors such as forming temperature, particle size distribution, and pitch/coke ratio affect the anode paste behavior when being formed.

Anode compaction may be a consequence of rearrangement of coarse coke particles that are influenced by the rheological properties of binder matrix. As coal-tar pitch is solid at room temperature, the rheological testing of pitch and binder matrix must be performed at elevated temperatures, introducing challenges like temperature variations, temperature gradients, and high working temperatures. Another challenge is the opaque nature of binder matrix and coarse particles. The absence of optical contrast prevents visualization of particle movement during compaction. It is therefore of great interest to develop methods to overcome challenges related to investigating rheological properties of binder matrix and anode paste behavior during compaction.

1.2 Aim of Work

The aim of this thesis was to investigate the rheological properties of fluid models to improve the understanding of anode paste behavior during compaction. Rheological properties of coal-tar pitch and binder matrix have previously been characterized at the process temperature of 178 °C as well as at 166 °C and 190 °C [10, 11]. Due to high process temperature, thermal gradients, and temperature variations related to working with pitch and binder matrix, fluid models with potentially similar rheological properties were researched at room temperature. Tracking the movement of particles in an anode paste during compaction cannot be done due to the lack of optic contrast between the binder matrix and coarse particles. Transparency of fluid models may therefore enable visualization of particle movement.

Chapter 2

Literature Review

2.1 Raw Materials in Anodes

2.1.1 Coke Particles

Calcined petroleum coke is the main constituent of green anodes with 60-75 % [4]. Green petroleum coke is a by-product of the distillation of raw petroleum. Before being used as a raw material in anodes, green petroleum coke must be heat treated by calcination to obtain the required thermal conductivity, increase grain strength and purity by the release of volatiles, and reduce electrical resistivity, air reactivity, and shrinking behavior during anode baking [12]. Rotary kiln calciners and rotary hearth calciners are generally used to calcine the green petroleum coke at temperatures from 1250 °C to 1350 °C [4]. Calcining also assures that the pores present have binder accessibility [13]. There are both open and closed type pores, whereas only the former is accessible to the binder. Coke with more open porosity than closed porosity is therefore favorable. Pore dimensions depend on multiple factors like the properties of raw petroleum and processing characteristics.

Table 2.1 shows the typical content of impurity elements in calcined petroleum coke [4]. The different impurity elements in the coke impact the anode properties and other aluminium production operations. Elements like sulfur,

Table 2.1: Ranges of impurities and target composition for good anodes, adapted from Keller and Sulger [4].

Element	Unit	Worldwide ranges	Targets for good anodes
S	%	0.5 - 3.0	≤ 2.2
V	ppm	20 - 350	≤ 220
Ni	ppm	40 - 250	≤ 130
Si	ppm	50 - 300	≤ 150
Fe	ppm	100 - 800	≤ 350
Na	ppm	100 - 1000	≤ 200
Ca	ppm	50 - 500	≤ 300

vanadium, nickel, sodium, calcium, and magnesium have an impact on the anode consumption while vanadium and phosphor affect the current efficiency. Vanadium, nickel, silicon, and iron affect the purity of aluminium metal. Sulfur reacts with oxygen in the air to SO_2, which should be limited from an environmental perspective.

Anodes used in the aluminium electrolysis usually have a lifetime of 25 days after which they are removed [14]. The spent anode butts are cleaned of electrolyte residues and crushed before being recycled. The anode butts represent the second largest constituent of green anodes with 20-25 % [4]. There are two categories in which anode butts are classified: soft and hard butts [8]. Soft butts have been more attacked during the electrolysis and will degrade the anode quality. The CO_2 gas formed at the anode will penetrate the soft butts, resulting in a weaker anode structure [4]. Hard butts will not be as susceptible to penetration. Similarly to calcined petroleum coke, there are pores present in the anode butts. Their dimensions depend on the anode properties prior to use in the electrolysis in addition to the degree of electrolyte contamination [15].

2.1.2 Pitch

Pitch is used as a binder in the anode paste and constitutes 13-15 % of green anodes [4]. Figure 2.1 shows the role of the binder pitch in an anode paste. Hulse [16] hypothesized that the main role of binder is to wet the coke particles by adsorption. The binder also penetrates the pores of coke

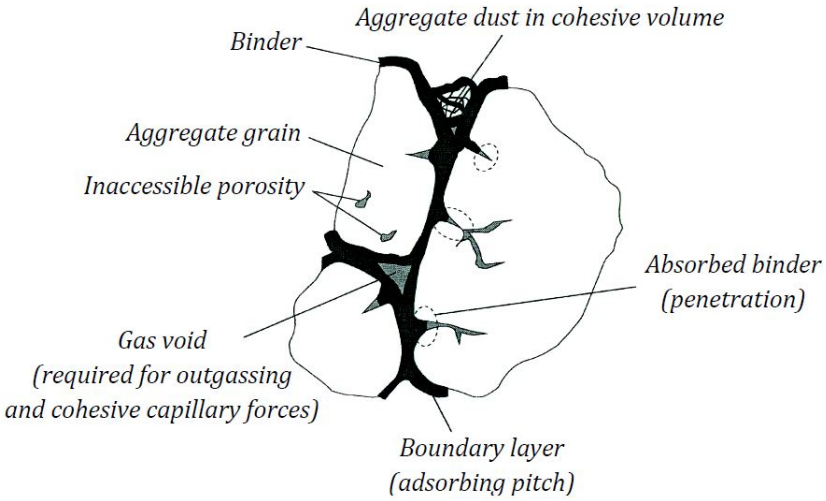

Figure 2.1: Pitch and coke aggregates [16].

particles and fills the space between wetted particles to cohere. Coal-tar pitch is the most common binder material in aluminium anode production and is a by-product from the production of metallurgical coke [4]. Metallurgical coke is used as a raw material for iron production and is made of coal that is transformed to coke through pyrolysis by being heat treated in ovens between 1100 and 1200 °C for 12-36 hours. Approximately 4 % of the charged coal produces coal-tar, which must be distilled to remove several components like napthalene, phenol, cresol, and creosote to obtain a pitch that can be used in anode production.

Pitch has a complex composition depending on the coal quality and processing, such as temperature and coking time [4]. A typical carbon content in coal-tar pitch used in anodes in aluminium industry is 93 wt. % [17]. Other elements include hydrogen (~4.5 wt. %), nitrogen (~1 wt. %), oxygen (~1 wt. %) and sulfur (~0.5 wt. %) presented as polycyclic aromatic hydrocarbons (PAHs) and heterocyclic compounds [4, 17]. In addition to the content of especially hydrogen, oxygen, sulfur and volatiles, pitch may be characterized by many other properties such as the following [18–20]:

- Softening point
- Coking value
- Viscosity

- Density
- Ash content
- Wetting ability
- Quinoline insolubles

The softening point describes the softening of pitch as pitch does not have a defined melting point, but a gradual transition from solid to a viscous fluid [21]. Coking value indicates how much carbon originating from pitch is likely to remain in the anode after baking [16]. As volatiles are released during baking, some pitch will be lost. Viscosity is a measure of the fluidity of the pitch and is a determining factor on how anode paste moves during processing. The ash content indicates the amount of impurity elements such as sulfur which should be limited in order to prevent SO_2 emissions during anode baking [16]. Quinoline insolubles are solid particles in pitch that are insoluble in quinoline solvent and affect the anode quality [16]. Branscomb et al. [22] found that increasing softening point, coking value, quinoline insolubles, and density of pitch result in increased anode apparent density and crushing strength, and decreased electrical resistivity. Typical ranges of coal-tar pitch properties are outlined in Table 2.2.

Pitch content is also crucial for the anode manufacturing [16]. Excessive pitching may cause crack formation (greater volatile release during baking), extreme shrinking and stub hole deformation [16, 23]. Insufficient pitch increases the anode porosity. The apparent density and mechanical properties

Table 2.2: Ranges of coal tar pitch properties, adapted from Keller and Sulger [4] and Hulse [16].

Property	Unit	Typical Range
Softening Point (Mettler)	°C	110 - 115
Coking Value	%	56 - 60
Viscosity at 160 °C	mPa·s	1200 - 2000
Viscosity at 180 °C	mPa·s	200 - 500
Density in Water	kg/dm^3	1.31 - 1.33
Ash content	%	0.1 - 0.3
Quinoline Insolubles	%	6 - 16

decrease as a consequence as well as increasing electrical resistivity [24]. There are multiple parameters determining the optimal pitch content, including [16]:

- Raw materials properties: porosity of coke particles and wettability of both coke particles and pitch.
- Paste recipe: coke particle size distribution, anode butt content and dust fineness and content. Anode pastes with high particle dispersity have a large total surface area, and more pitch is thus needed to obtain the maximum density.
- Manufacturing process: the paste operation affects how the pitch is distributed in the paste. Inadequate paste processing results in a heterogeneous paste.

2.1.3 Particle Granulometry

Aggregates and fines in the anode are mainly made of calcined petroleum coke with a smaller share of recycled anode butts. The size range of large aggregates are larger than 0.15 mm and smaller than 9.5 mm, and the fine particles are smaller than 0.15 mm [7]. Particle size distribution affects density, pore size distribution, electrical resistivity, and other anode properties [8,13]. The density increases with an increasing amount of fine particles due to the contribution of fine particles to fill inter-particle voids. Fine particles also have lower porosity than coarse particles as the latter tend to break in porous regions when being ground to smaller particles, thus decreasing the porosity of the coke fraction [13,25]. A wide range of particle sizes also increases the density as smaller particles fill inter-particle space of a wide range space sizes without increasing the volume [25,26].

Vidvei et al. [27] studied the dispersity and content of fine coke particles. Electrical resistivity was found to decrease with increasing dispersity of fine particles towards 40-60 % below 75 μm. Rørvik et al. [28] had similar findings by image analysis. It was revealed that the amount of fine particles below 75 μm increases with increasing milling times, resulting in smaller inter-particle distance between coke grains, thinner layers of pitch between

particles and decreased electrical resistivity.

Excessive dispersity and content of fine coke particles require more binder pitch, and the resulting anode paste may be difficult to process [13]. Fine particles have larger surface areas, and more pitch is necessary to completely wet the particle surface and avoid the effects of under-pitching [24]. However, high amounts of pitch can lead to an uneven pitch distribution and cracks during baking [29]. Other anode properties like air permeability and thermal shock resistance also decrease with increased particle dispersity and content [13, 29]. Not all anode properties can be maximized by specific particle size distribution. An optimum range of particle sizes and amounts is therefore used to obtain the highest quality possible.

2.2 Anode Manufacturing

2.2.1 Paste Plant

The anode paste is produced in a paste plant where the anode constituents are treated [4]. Generally, anode plants use more than one type of coke due to the variations in coke quality and increasing aluminium production [30]. To avoid large variations in anode quality and properties, different coke types are blended to the optimal recipe. The coke blend is crushed before being sieved into size fractions according to the anode specifications requested by the producer [31]. A ball mill is used to grind coke to the smallest size fraction. The required portion of different sizes is added to the dry aggregate recipe that is preheated before being mixed with the pitch to avoid the pitch to solidify [31]. The fine coke particles and pitch mix to a binder matrix, which surrounds the coarse coke particles and enters into their pores.

Parameters such as power, time, and temperature are important in determining the quality of the mixing and the resulting anode paste quality [32–34]. Optimal mixing should yield a homogeneous distribution of dry aggregate and binder pitch. The porosity should also be minimized to achieve improved density and thermal shock resistance. Azari [8] found that the most efficient mixing temperature was at 178 °C for a mixing time of

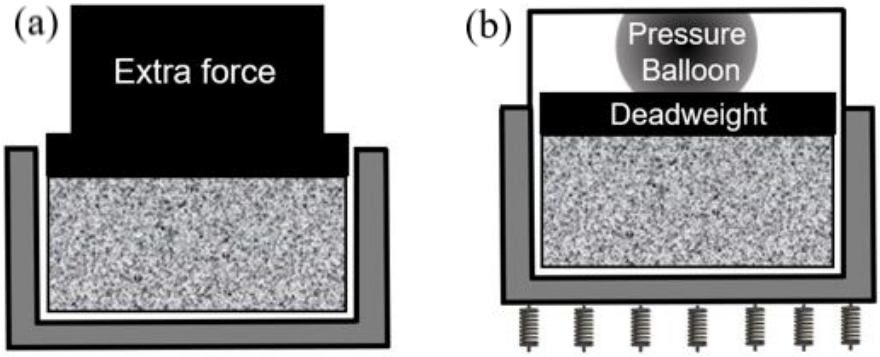

Figure 2.2: Illustration of (a) hydraulic press and (b) vibro-compactor [36].

10 minutes. 178 °C was also the same as the temperature used in commercial paste plants, which is normally 60-70 °C above the softening point of binder pitch.

The two different methods of anode paste compaction commercially used today are hydraulic pressing and vibro-compaction, illustrated in Figure 2.2 [35]. Anode paste is formed into blocks with stub holes for later rodding in the electrolysis. The pressing method requires pressure between 100 and 500 bar with a forming time of between 30 and 90 seconds [35]. The vibro-compactor may have lower throughput than the hydraulic press due to longer forming times. Both methods can achieve similar apparent density. However, there is a move towards vibro-compaction [35]. Compacted anodes have higher air permeability than pressed anodes, but lower electrical resistance, higher strength values, and much lower pressure. According to Hulse [35], the pressed anodes are sensitive to parameters influencing paste elasticity and insensitive to those influencing paste viscosity. The opposite is true for vibro-compacted anodes.

Major problems encountered due to poor anode compaction include low anode density, density gradients, high permeability, small anode cracks with a resulting increase in electrical resistivity and large anode cracks that may cause anode failure [38]. Figure 2.3 shows a CT-image of a prebaked anode with red circles around horizontal cracks. There are areas especially pronounced below stub holes with high density and other areas with low density.

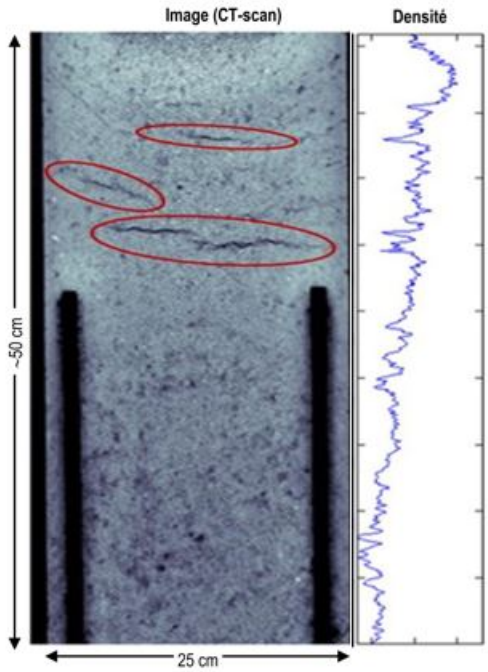

Figure 2.3: CT-image of a prebaked anode, adapted from Thibodeau [37].

The final step in making green anodes is anode cooling to avoid deformation after forming [4]. The anodes can the cooled by being submerged in or sprayed with water, or by air. To prevent thermal stresses that can cause cracks, the temperature difference between the water and the formed anode should be lowered by increasing the water temperature to approximately 70 °C. Anodes that are formed at higher temperatures by a vibro-compactor require being submerged in water, while anodes formed by a hydraulic press at lower temperatures may be cooled by air. If the anodes are quenched, the anodes can have compressive stresses and tension in the surface and core, respectively. When the anodes are heated during baking, these stresses may aggravate and cause cracks in the baked anodes. Crack formation can also occur due to thermal shock if the green anodes are taken from storage below 0 °C directly to baking at high temperatures.

2.2.2 Anode Baking

The anode baking furnace is built inside a shell of concrete with sections divided into two rows [39]. In the two rows, each section is attached to a headwall on both sides with openings for connection to an exhaust. A total

of approximately 16 sections comprises a fire group, and each of the sections has a maximum of eight pits, where green anodes are stacked. Figure 2.4 shows an illustration of a section with pits separated by flue walls. The anodes are covered with packing coke for mechanical support as the pitch softens, and to prevent oxidation by airburn. The pits are separated by flue walls in which the flue gas travels to heat up and cool down the anodes [5]. The exhaust connects the baking furnace to a gas treatment plant, producing an under pressure for the gas to travel through flue walls. During heating, the coal tar pitch cracks, resulting in the escape of volatiles through gaps in the flue wall due to the under pressure produced by the gas treatment plant. Volatile hydrocarbons will be combusted, contributing to the heating of the furnace. The heating gradient must be controlled and not exceed 14 °C/h as a heating gradient that is too high will cause excessive cracking of the anodes due to a too rapid release of volatiles [39].

The green anodes and packing coke are loaded into the pits before baking [39]. Heat is generated by the combustion of gas from burner ramps located at the top of the flue walls in an open top furnace and at the top of the section

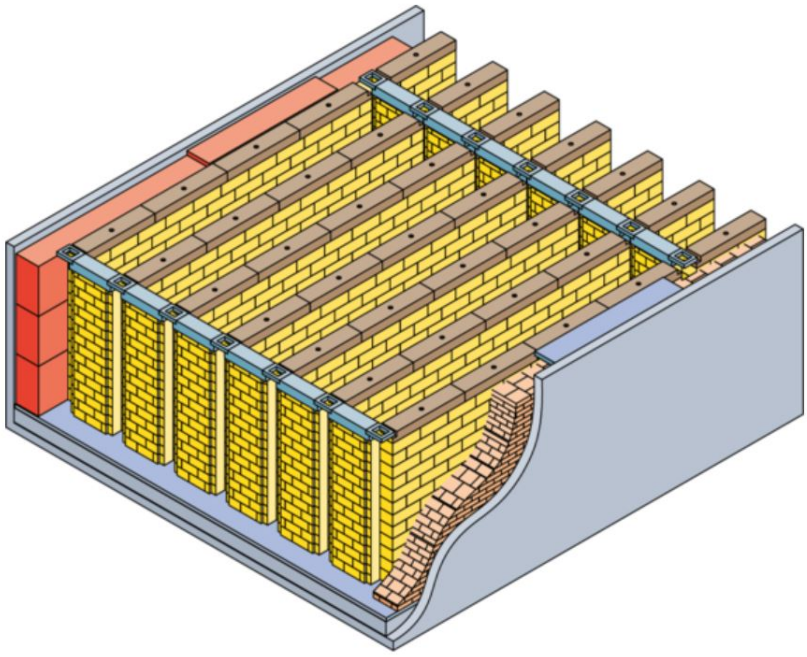

Figure 2.4: Illustration of an anode baking furnace with refractory walls and pits [40].

covers in a closed top furnace. The anodes are cooled down by fans after baking. Burner ramps, exhaust manifold, and cooler ramps are moved from one section to the next every 22-28 hours [5]. A complete firing cycle lasts between 14 and 17 days, depending on the duration of the firing periods. The first part of the firing cycle is pre-heating of the section at 200-600 °C in three periods [39]. Most of the volatiles are released in the pre-heating zone. Then the section is baked at temperatures up to the maximum temperature of 1200-1300 °C. Pitch completely transforms to coke in the temperature range 600-900 °C and anode properties are defined at 1050-1150 °C. Finally, the baked anodes are cooled down and unloaded from the pits.

2.3 Rheological Properties

2.3.1 Rheology of Fluids and Suspensions

For fluids that are Newtonian, the viscosity (μ) is independent of shear rate ($\dot{\gamma}$) and remain constant at constant temperature and pressure [41]. The shear stress is linearly proportional to the shear rate accordingly:

$$\tau = \mu\dot{\gamma} \tag{2.1}$$

The viscosity of real fluids is not always constant and depends on properties such as the shear rate, temperature, pressure, and time [41]. The addition of suspended particles can also change the viscosity.

There have been several studies on the rheology of suspensions as a function of shear stress [41]. If the base fluid is Newtonian in the relevant shear range, the suspensions can be expected to have Newtonian, shear-thickening, or shear-thinning behavior. Shear-thinning is a common phenomenon where the viscosity decreases with increasing shear rate. Shear-thickening is the increase in viscosity with increasing shear rate. Figure 2.5 (a) shows shear stress as a function of shear rate and Figure 2.5 (b) shows the viscosity as a function of shear rate for Newtonian, shear-thinning, and shear-thickening materials. If the viscosity is not constant, Equation 2.1 can be modified to

the power-law:

$$\tau = \kappa \dot{\gamma}^n \tag{2.2}$$

where κ is the consistency index and n is the power index. n is equal to unity for Newtonian behavior, lower than unity for shear-thinning behavior and higher than unity for shear-thickening behavior. There can also be an appearant yield stress in the fluid, below which flow does not exist under the experimental boundaries [41]. The concentration of suspensions where yield stress has been detected in previous experiments have mostly exceeded a volume fraction of 0.5 [42]. It has been argued by Barnes [43] that all fluids flow under shear, but is undetectible in certain experiments. Some fluids even demonstrate creep under stresses below the yield stress. However, it is common to use different models to describe experimental data from a limited shear rate including a yield stress parameter as Equations 2.3 [44] and 2.4 [45].

$$\tau = \tau_0 + \mu_p \dot{\gamma} \tag{2.3}$$

$$\tau = \tau_0 + \kappa \dot{\gamma}^n \tag{2.4}$$

where τ_0 is the yield stress and μ_p is the plastic viscosity (both constant).

When particles are suspended in a fluid, there are three different forces acting on the particles [41]. The first is colloidal forces from the interaction

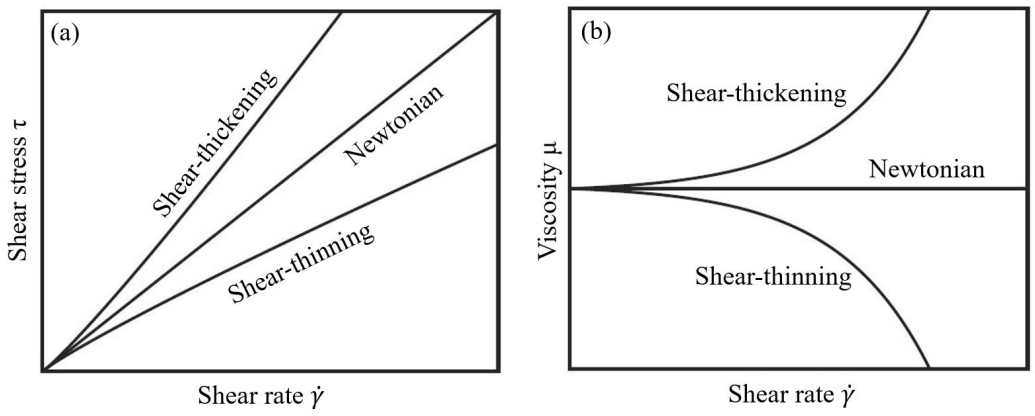

Figure 2.5: Illustration of (a) shear stress and (b) viscosity as a function of shear rate for Newtonian, shear-thinning, and shear-thickening fluids.

between particles causing inter-particle repulsion or attraction. The second is Brownian (thermal) forces that cause random motion of particles from collisions with fluid molecules (Brownian motion). Finally, there are viscous forces on the particles from the surrounding fluid. Which force is dominating depends on shear rate and other parameters like temperature, base fluid properties, and particle properties.

Wagner and Brady [46] explained in a review, the transition in a concentrated suspension with shear rate, illustrated in Figure 2.6. The suspension is at equilibrium with constant viscosity at low shear rates as Brownian motion dominates the flow induced motion to restore the random particle distribution. When the shear rate increases to a point when the colloidal forces dominate, particles organize and align. The viscosity of the suspension decreases as the particles move past each other more efficiently, and the suspension has shear-thinning behavior. The resulting structure depends on whether the total forces are attractive or repulsive [41]. If the shear rate is further increased, there is a Newtonian plateau before the shear rate reaches a critical value where shear-thickening may occur as the viscosity starts to

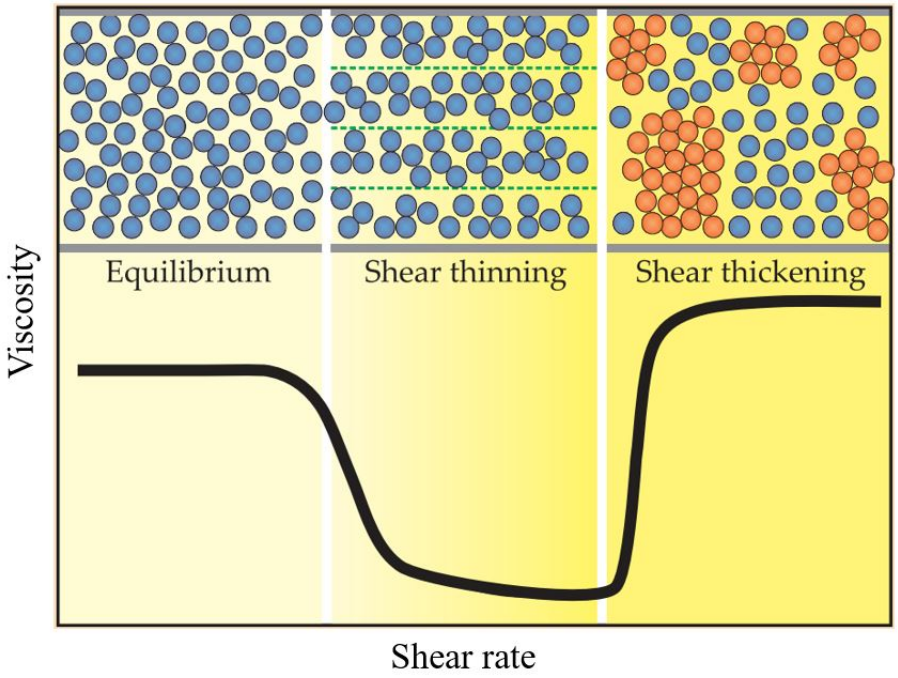

Figure 2.6: Illustration of the transition in a suspension with viscosity as a function of shear rate, adapted from Wagner and Brady [46].

increase. It has been indicated by some studies that shear-thinning will resume after the shear-thickening region if there is no fracture [47,48].

Particle interaction through attractive or repulsive forces and the presence of Brownian motion contribute to determining the nature of interaction [49]. The dominance of Brownian motion depends on the particle size and is generally negligible for particles larger than micrometer size. If the total interaction force is attractive, aggregation of particles controls the suspensions. An important phenomenon is the breakage of aggregated particles when shear is applied, resulting in shear-thinning behavior. There is a steady state during equilibrium when the attractive and shearing forces cancel each other out.

Repulsive interaction forces may cause shear-thickening behavior. Hoffman [48] suggested that the origin of the shear-thickening behavior observed in polymeric resins suspensions with particle volume fractions above 0.5, was due to an ordered-disordered transition in the particle microstructure. By white light diffraction, ordered strings and layers were observed at low shear rates that broke at a higher critical shear rate. The resulting structure was assumed to be more inclined to jam with an increased viscosity as a consequence. These findings were challenged by studies suggesting that order-disorder transition was not necessary for shear-thickening behavior, due to the absence of layer formation [50–55]. Hydro-cluster formation during shear-thickening is the proposed mechanism.

Deviation from Newtonian behavior depends on many parameters like particle size, particle size distribution, volume fraction of particles, tendency to agglomerate, deformation operation, etc. [47]. Lootens et al. [56] found that the power index from fitting results with the power law (Equation 2.2) decreased with decreasing particle size in the range between 0.1 and 2.5 μm in silica slurries. The decrease of the power index demonstrate increasing shear-thinning behavior, and it was proposed that aggregated small particles are more easily broken during low shear rates than aggregated large particles. The influence of particle size on the power index at higher shear rates in the shear-thickening regime was harder to predict. Van der Werff and de Kruif [57] did not find the same correlation between particle size

and shear-thinning for particles smaller than a micrometer and stated that the most important parameter was the volume fraction. Only a small effect of particle size on the shear-thinning behavior was observed by Tsai and Zammouri [58] who studied suspensions with particles of sizes 2-150 μm. The viscosity was however considerably higher for a suspension with 6 μm particles than a suspension with 78 μm particles.

Particle size distribution is another important parameter influencing the rheological behavior of suspensions. A wide particle size distribution increases the maximum volume packing and the critical shear rate for the onset of the shear-thickening regime as a consequence [47]. If the volume fraction is less than approximately 0.3, then shear-thickening behavior is rarely visible [46, 59]. The volume fraction required for the onset of the shear-thickening regime varies greatly with multiple parameters. A volume fraction of approximately 0.5 has been reported as a typical value where shear-thickening can be observed [46, 47, 59], while others report absence of shear-thickening independent of volume fraction [57]. Due to the many parameters governing the rheological properties of suspensions, it may be hard to predict the behavior of materials based solely on chosen parameters such as shear rate and volume fraction.

2.3.2 Suspension Models

Many attempts have been made to model the viscosity as depending on the concentration for suspensions [49]. Einstein [60,61] attempted to predict the viscosity of dilute suspensions and showed that single particles increased the viscosity of a fluid as a function of volume fraction:

$$\mu_r = 1 + 2.5\phi \tag{2.5}$$

where μ_r is the ratio of the effective viscosity of the suspension, and the viscosity of the suspending medium and ϕ is the volume fraction of suspensions. There is no consideration of particle size or position in the model as it neglects the complicated interaction with other particles. A modification of Einstein's equation, including a second-order term of ϕ to describe

inter-particle interaction, has been proposed:

$$\mu_r = 1 + 2.5\phi + K\phi^2 \tag{2.6}$$

where K is a coefficient. Reported values of K from the literature are 4.375 [62, 63], 14.1 [64] and 6.2 [65]. The suspension models above are only valid for dilute suspensions up to a volume fraction of approximately 0.1.

Models relating the influence of particle concentration and the maximum possible packing volume fraction on the viscosity of suspensions have been proposed [41]. The suspension will eventually ”jam” with all particles having a continuous contact and flow will stop, causing the viscosity to rise towards infinity. The volume fraction at which the suspension ”jam” is the maximum possible packing volume fraction. Equations 2.7-2.11 presents models for viscosity of suspensions based on maximum packing fraction of particles [66–70]:

$$\mu_r = \left(1 - \frac{\phi}{\phi_m}\right)^{-2.5\phi_m} \tag{2.7}$$

$$\mu_r = \left(1 - \frac{\phi}{\phi_m}\right)^{-2} \tag{2.8}$$

$$\mu_r = \left(1 - \frac{\phi}{1 - \phi/\phi_m}\right)^{2} \tag{2.9}$$

$$\mu_r = 1 + 2.5\phi\left(1 - \frac{\phi}{\phi_m}\right)^{-1} + 0.1\left(\frac{\phi}{\phi_m}\right)^{2}\left(1 - \frac{\phi}{\phi_m}\right)^{-2} \tag{2.10}$$

$$\mu_r = \frac{e^{-2.34\phi}}{(1 - \phi/\phi_m)^3} \tag{2.11}$$

where ϕ_m is the maximum possible packing volume fraction and is dependent on the packing-type, particle size distribution, and particle shape [41]. The maximum packing fraction for random close packing is 0.637. As pre-

viously mentioned, a wide particle size distribution increases the maximum packing fraction. Non-spherical particles will decrease the maximum packing fraction due to inadequate space-filling abilities.

2.3.3 Viscoelasticity

Viscoelastic materials simultaneously have both viscous and elastic properties [41]. Elastic materials have the capacity to store mechanical energy without dissipation, while viscous materials dissipate energy without storing it. Viscoelastic materials can therefore both dissipate and store mechanical energy. If the material is subjected to oscillation strain, storage and loss modulus as a function of angular frequency can be found. The storage (elastic) modulus represents the energy stored in the material and the loss (viscous) modulus represents the energy dissipated in the material.

The elastic properties of viscoelastic suspensions have been studied in different fluids. Aral and Kaylon [71] found that the storage modulus increased with increasing volume fraction up to 0.6 for a non-Newtonian silicone oil with hollow glass beads with a diameter of 12 μm. When the volume fraction was higher than ~0.3 at low angular frequencies, there was a significant increase in storage modulus. For volume fractions higher than ~0.5 both the storage and loss modulus reached a plateau at low angular frequencies, suggesting increased relaxation times for the elastic effects to decay and development of yield stress with increasing volume fractions. Other studies have reported the increase in storage modulus with increasing volume fractions with particles ranging from 4 to 80 μm in diameter [72, 73]. However, the reported increase differs and is hard to predict, due to the complex nature of fluids with and without suspensions.

2.3.4 Anode Paste, Binder Matrix and Pitch

Hulse [9] studied the rheological properties of anode paste and hypothezised that the pitch-aggregate mixture was granulo-viscoelastic and dependent on temperature. At high temperatures, the paste is mainly viscous. When the temperature decreases, the paste becomes more stiff and elastic. At low temperatures and high elastic behavior, the shape of the paste remains the

same before and after load. The anode paste is also susceptible to shear rate or frequency. The rheological properties of the anode paste are important during paste processing and especially during mixing and compaction. As mentioned previously, the shear rate is a major factor determining the viscosity of a material and depending on the mixer used in the paste plant the average shear rate can range from up to 80 1/s for a sigma blade to up to 1000 1/s for a kneader [9]. Vidvei et al. [27] found that the viscosity of an anode paste reaches a minimum when increasing the dispersity of fine particles to approximately 60 % below 75 μm. The viscosity minimum at ~60 % nearly corresponds to the density maximum for vibro-compacted paste. Increasing the total fine particle content increased the minimum viscosity.

Binder matrix is the deformable phase in the anode paste, surrounding coarse coke particles. Gildebrandt et al. [74,75], Kravtsova et al. [76] and Vershinina et al. [77] studied the influence of temperature, fine coke particle size and fine coke particle content on the viscosity of binder matrix. The viscosity of the binder matrix increases with both decreasing temperatures as the viscosity of the viscous medium (pitch) increases, and decreasing particle size. A binder matrix system with fine coke particles smaller than 74 μm had a low increase in viscosity with increasing particle content up to 50 wt. % and a significant increase when the particle content exceeded 50 wt. %. Hulse [9] and Kravtsova et al. [76] suggest that this effect is dependent on particle interaction, number of particle contact points, and the pitch layer thickness on the particle surface. Figure 2.7 shows the difference between a loose configuration with lubricated contacts at low particle concentration and a closed configuration with direct inter-particle contact at high concentration [9]. The number of particle contact points increases with decreasing fine coke particle size and the pitch layer thickness decreases. Thus, particles interact through friction at high concentration while the interaction is hydrodynamic at low concentration, with the former incrementing the strength of the pitch-coke system [76].

Both elastic and viscous behavior contribute to the deformation and compaction of the anode paste [9]. Elasticity and viscosity of the anode paste

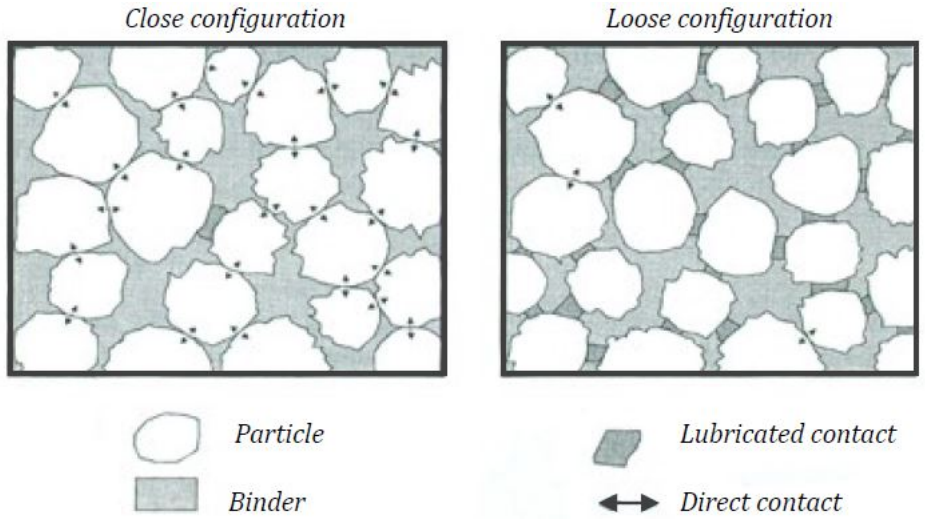

Figure 2.7: Illustration of the anode structure [9].

increase with decreasing fine coke particle size and increasing fine coke particle content as the area of the particle surface increase due to the increase of phase volume (space taken by particles) [9]. The viscous component of the paste will increase as the viscosity decrease. Increased temperature and pitch content contribute to decreasing the viscosity. The elastic component increase with increasing coke concentration and fineness of particles. A balance between the two components should be obtained for optimal paste rheology during mixing and compaction.

Mollaabbasi et al. [11] studied the rheological properties of pitch and binder matrix with different concentrations of fine coke particles up to the industrial concentration of 60 wt. % as an extension of previous work on pitch and binder matrix with fine coke particle concentrations up to 15 wt. % [10]. Three temperatures were used: 166 °C, 178 °C and 190 °C. Calcined petroleum coke and coal tar pitch with densities of 2.057 g/cm^3 and 1.31 g/cm^3, respectively, were used to produce twelve binder matrix samples. Table 2.3 shows the fine particle size distribution

Table 2.3: Size distribution of fine particles, adapted from Mollabbasi et al. [10].

Size range (μm)	+150	-150+106	-106+75	-75+53	-53+38	-38
wt. %	3.1	11.5	15.6	18.7	14.6	36.5

with a Blaine number of 4000 cm^2/g. The Blaine number (BN) is an indication of specific surface area in the industry and determines the fineness of coke particles. A Discovery Hybrid Rheometer (DHR-3) with two 20 mm Peltier parallel plates with a gap thickness of 1000 μm was used to perform rotational and oscillation tests. Only samples with up to 35 wt. % were tested rotationally due to the limitation of this method testing suspensions with high concentrations. Oscillation testing was performed on all samples.

The power law model (Equation 2.2) was used to correlate the results from rotational testing to the rheological behavior of pitch and binder matrix and Table 2.4 shows the consistency and power index for concentrations of fine particles up to 35 wt. % at the three temperatures [11]. The power index of pitch is close to unity for all the tested temperatures, revealing that pitch is a Newtonian fluid in this temperature and shear rate range. The power index generally decreases with increasing concentration for all temperatures and increases with increasing temperature for most concentrations. These results show shear-thinning behavior and can also be seen in Figure 2.8 that shows shear stress as a function of shear rate at the three temperatures. The shear stress increases with decreasing temperature, meaning that the viscosity of the binder matrix decreases with increasing temperature.

Table 2.4: Consistency and power index for pitch and binder matrix from the power law at three temperatures, adapted from Mollabbasi et al. [11].

Conc. (wt. %)	0	5	10	15	20	25	30	35
				166 °C				
n (-)	1.00	0.93	0.93	0.91	0.90	0.90	0.90	0.87
κ ($Pa{\cdot}s^n$)	7.27	12.64	14.68	19.76	19.88	25.97	31.44	66.66
				178 °C				
n (-)	1.00	0.94	0.94	0.92	0.92	0.91	0.90	0.89
κ ($Pa{\cdot}s^n$)	2.55	4.96	6.09	6.99	7.59	10.24	12.62	18.80
				190 °C				
n (-)	1.00	0.96	0.94	0.93	0.93	0.92	0.91	0.90
κ ($Pa{\cdot}s^n$)	1.31	2.44	3.27	3.51	3.57	5.17	6.29	9.67

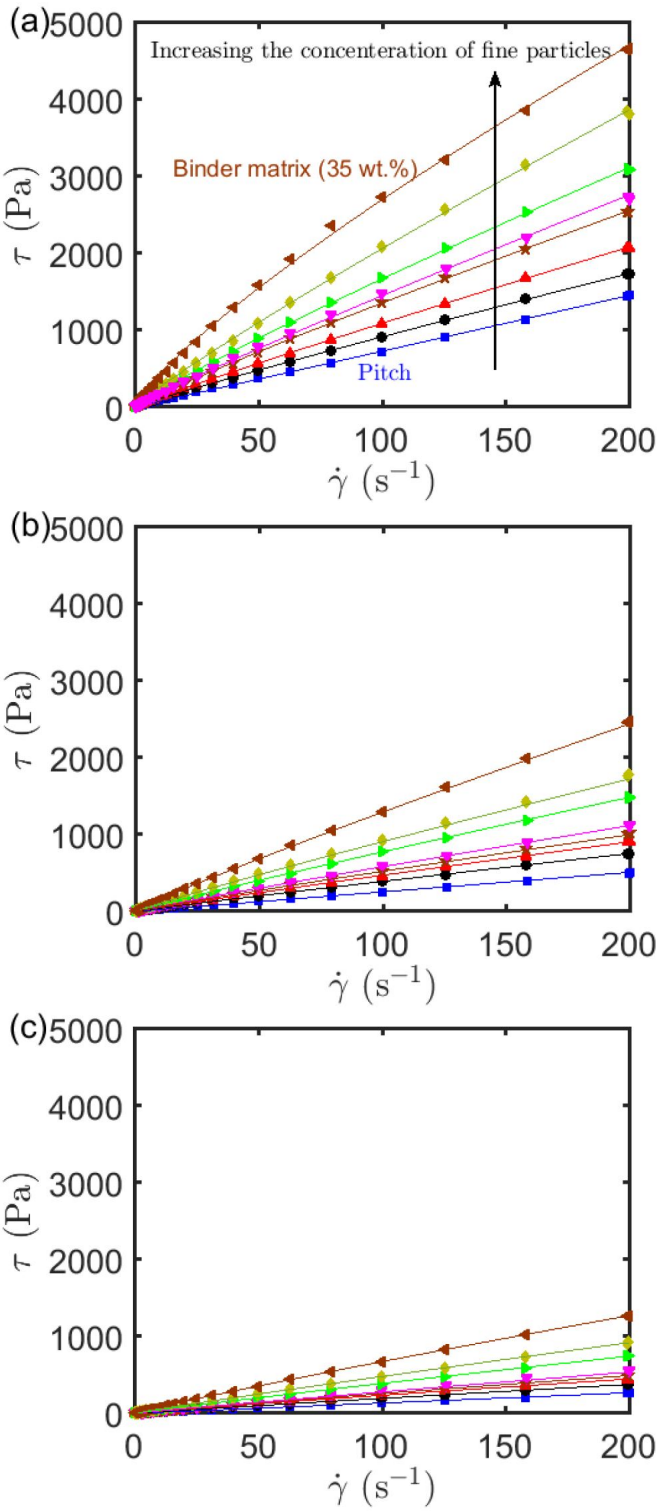

Figure 2.8: Shear stress as a function of shear rate for binder matrix with fine particles concentrations increasing from 0 to 35 wt. % according to the arrow direction at (a) 166 °C, (b) 178 °C and (c) 190 °C [11].

Figure 2.9 shows the storage modulus as a function of angular frequency for binder matrix with all concentrations of fine particles for three different temperatures [11]. The elastic properties of the binder matrix increase with increasing particle concentration and decreasing temperature for all particle concentrations.

The loss modulus as a function of angular frequency is shown in Figure 2.10 with all concentrations of fine particles at three different temperatures [11]. The viscous properties of the binder matrix increase with increasing particle concentration and decreasing temperature for all particle concentrations. Both storage and loss modulus results collaborate that binder matrix is visco-elastic and that the viscous and elastic components increase with increasing concentration of fine particles.

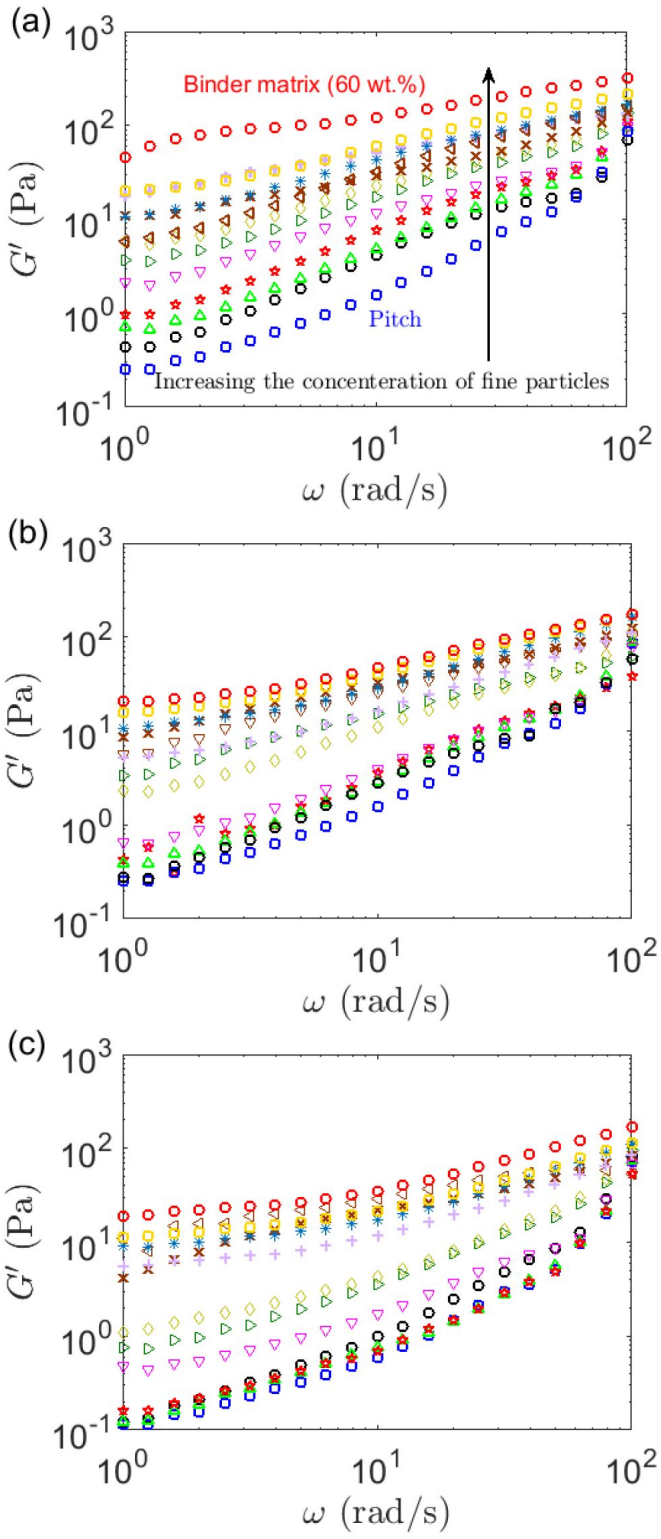

Figure 2.9: Storage modulus as a function of angular frequency for binder matrix with fine particles concentrations increasing from 0 to 60 wt. % according to the arrow direction at (a) 166 °C, (b) 178 °C and (c) 190 °C [11].

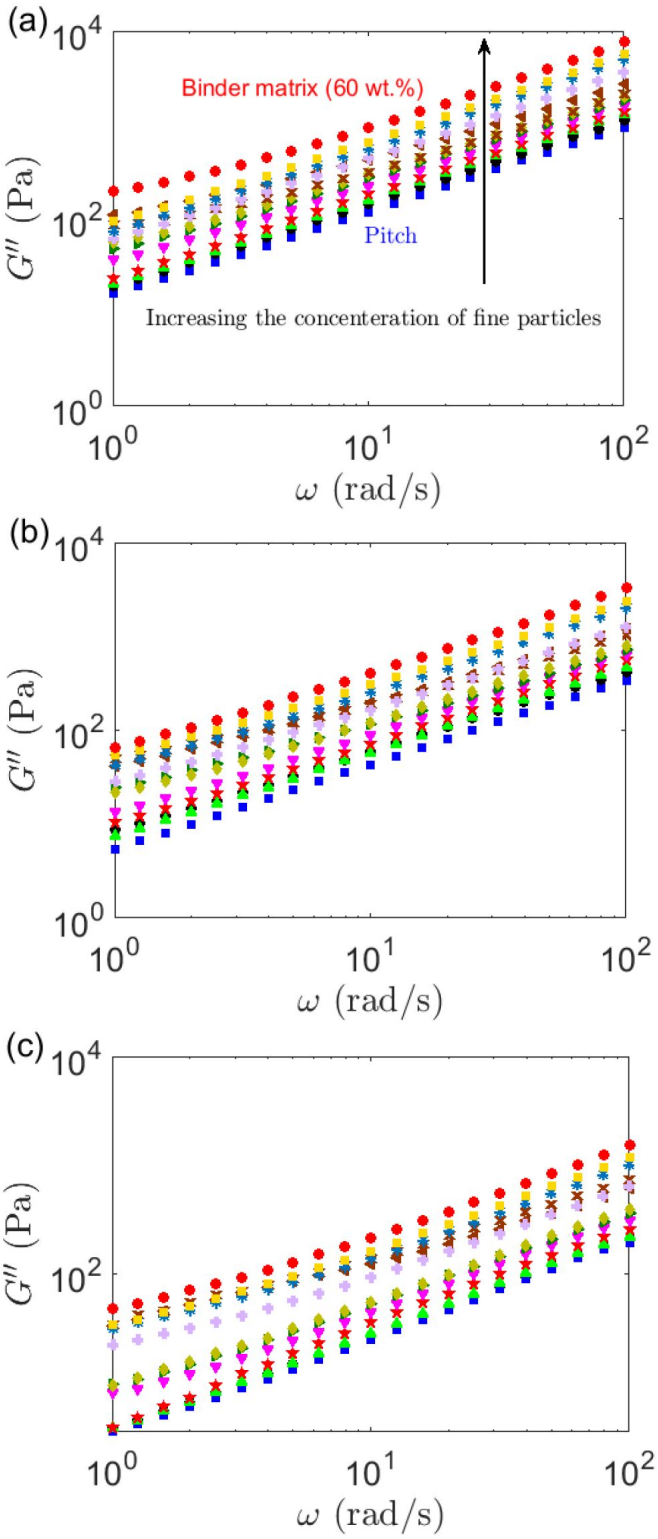

Figure 2.10: Loss modulus as a function of angular frequency for binder matrix with fine particles concentrations increasing from 0 to 60 wt. % according to the arrow direction at (a) 166 °C, (b) 178 °C and (c) 190 °C [11].

Chapter 3

Method

3.1 Materials

3.1.1 Silicone Oil and Coke Particles

One sample of silicone oil and three samples of silicone oil with fine coke particles were prepared prior to project initiation. The first sample was pure silicone oil with no addition of fine coke particles. The other three samples had additions of 5 %, 10 % and 15 % fine coke particles. All four samples were stored in plastic containers with a closed lid.

3.1.2 Xanthan Solution

Ten samples of Xanthan solution between 100 and 10000 ppm were prepared at room temperature. Xanthan gum powder was weighted according to the concentration and added to a glass cylinder. The powder was dissolved in 4-6 drops of glycerine to speed up the mixing process. Distilled water was added to the sample for a total weight of 40 g. Samples with a concentration of up to 3000 ppm were stirred by a magnetic stirrer for 15-30 minutes. Due to the limited reach of the magnetic stirrer in more concentrated and viscous samples, samples from 5000 ppm up to 10000 ppm were manually stirred until all agglomerated powder flocs were visibly dissolved. To allow bubbles generated from stirring to dissipate, the samples were rested between 90 and

120 minutes under a cover.

3.1.3 Carbopol Gel

Four samples of Carbopol (polyacrylic acid) gel from a Carbomer 940 was prepared at room temperature, two samples in the low concentration range with 0.2 % and 0.3 % and two samples in the high concentration range with 1.6 % and 2.5 %. Carbopol powder was sieved and weighted in a glass cylinder before distilled water was added to a total weight of 40 g. The low concentration samples were mixed with a magnetic stirrer, while the two high concentration samples were mixed manually until all agglomerated powder flocs were visibly dissolved. All samples rested under cover for approximately 30 minutes for bubbles to dissipate.

3.1.4 PEO

Five samples of $9{\cdot}10^5$ g/mol PEO (polyethylene oxide) was prepared at room temperature with concentrations from 3 % to 7.4 %. Due to long stirring times, a larger 7.4 % sample was prepared by weighing PEO powder in a glass cylinder, adding distilled water to a total weight of 80 g and stirring manually until all agglomerated powder flocs were visibly dissolved. The other four samples of lower concentration were made by diluting the 7.4 % sample with distilled water. All samples were stirred by a magnetic stirrer and rested for 90-120 minutes under a cover for bubbles to dissipate. Figure 3.1 shows a glass cylinder with the 7.4 % sample.

3.2 Rheological Measurement

The rheological properties of fluid models were characterized by a Discovery Hybrid Rheometer (DHR-3) that can be seen in Figure 3.2. TA Instruments TRIOS was the instrument control software used. To calibrate the rheometer, instrument inertia was determined and accepted in the range from 20.5 to 21.5 μNms^2 and no more than a 10 % difference from the original inertia value. A 20 mm Peltier parallel plate geometry was used and calibrated by determining the geometry inertia and bearing friction correction. The

temperature was set to 25 °C, and the gap thickness was set to 1000 µm for all measurements.

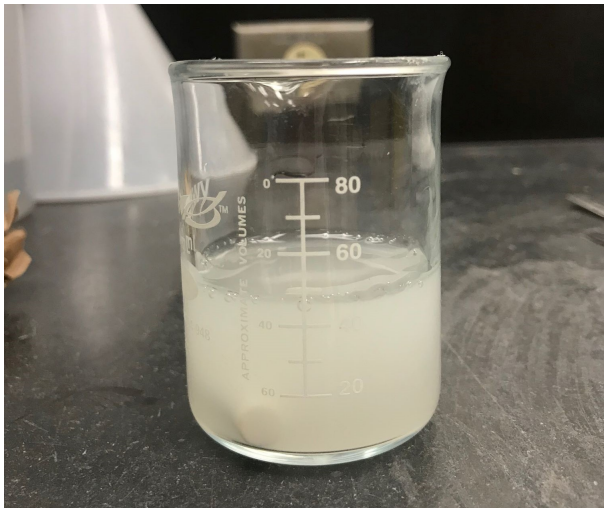

Figure 3.1: Glass cylinder with PEO solution.

Figure 3.2: Discovery Hybrid Rheometer (DHR-3) with a 20 mm Peltier parallel plate geometry lowered to a 1000 µm gap thickness.

Rotational testing (flow sweep) was used to measure the viscosity and shear stress as a function of shear rate for all fluid models. The shear rates used ranged from 0.5 to 100 1/s. Oscillation testing (frequency sweep) was used to measure the viscoelastic properties, namely the storage and loss modulus as a function of angular frequency for Xanthan solution, Carbopol gel and PEO solution. The constant strain amplitude for Carbopol was set to 1 % based on previous experience working on Carbopol. Amplitude sweeps were performed at the highest concentrations of Xanthan solution and PEO solution at a constant angular frequency of 1 rad/s.

Chapter 4

Results

4.1 Fluid Models

4.1.1 Silicone Oil and Coke Particles

The shear stress (τ) of silicone oil and silicone oil with three different concentrations of fine coke particles (5, 10 and 15 %) as a function of shear rate ($\dot{\gamma}$) from rotational testing is presented in Figure 4.1. There is linear relationship between the shear stress and shear rate for all samples, demonstrating a Newtonian behavior. This assessment is supported by the nearly constant viscosity for all four samples, as seen in Figure 4.2. The viscosity of silicone oil with 0, 5, 10 and 15 % fine coke particles were approximately 2.72, 2.87, 2.97 and 3.01 Pa·s, respectively. No apparent yield stress was detected for any sample. The shear stress and the viscosity increase with increasing fine particle content. The power and consistency index from curve fitting of the power law (Equation 2.2) are presented in Table 4.1. The power index

Table 4.1: Power index and consistency index from curve fitting of the power law (Equation 2.2) for four different concentrations of fine coke particles in silicone oil.

Conc. (%)	0	5	10	15
n (-)	1	1	1	1
κ (Pa·s^n)	2.75	2.91	3.01	3.05

is equal to unity for all samples, and the consistency index increase with increasing fine particle content as expected from the previous results.

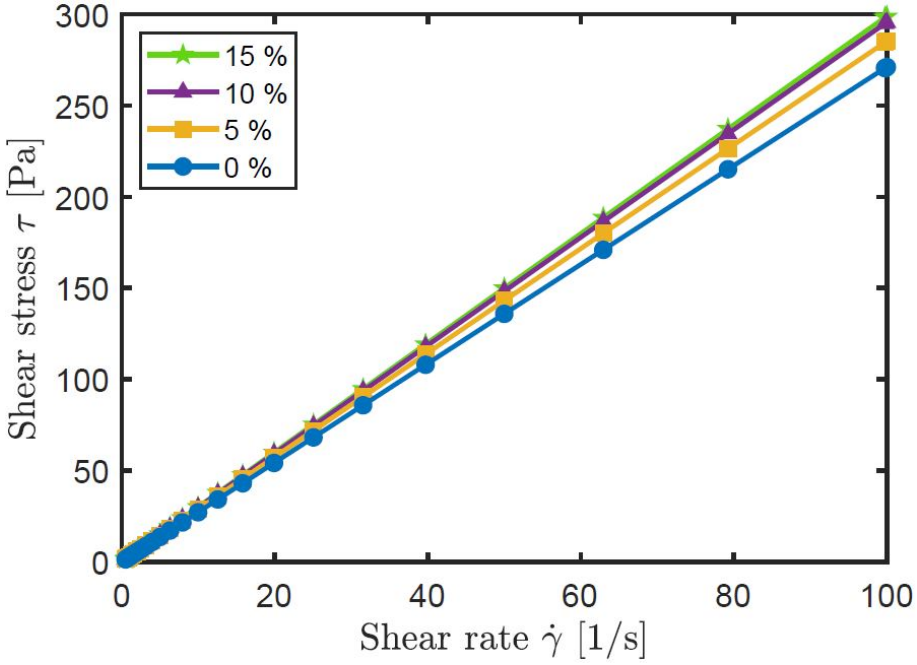

Figure 4.1: Shear stress of silicone oil with four different concentrations of fine coke particles as a function of shear rate (0 % (●), 5 % (■), 10 % (▲) and 15 % (★)).

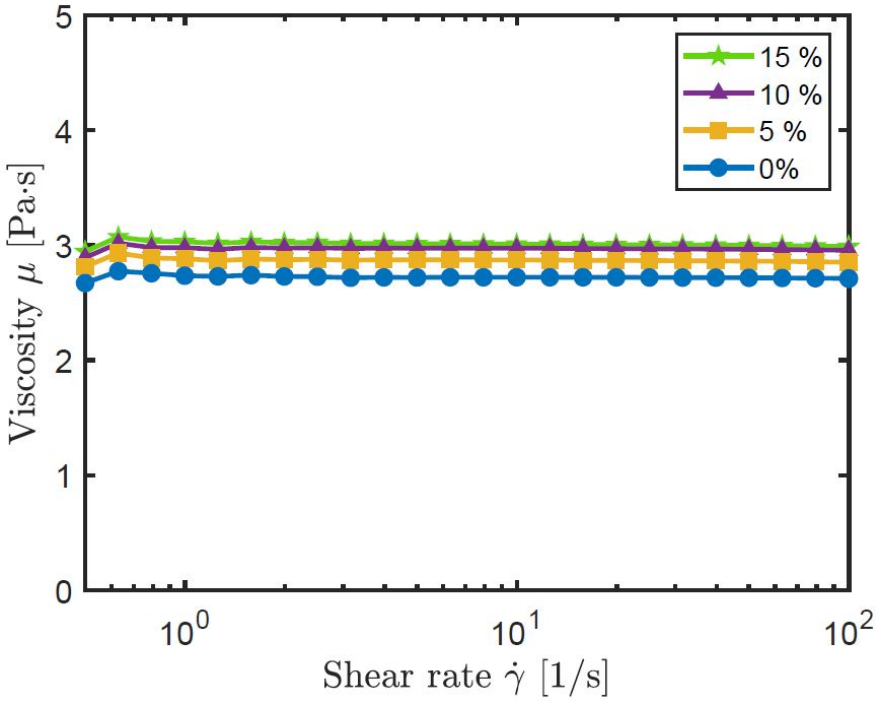

Figure 4.2: Viscosity of silicone oil with four different concentrations of fine coke particles as a function of shear rate (0 % (●), 5 % (■), 10 % (▲) and 15 % (★)).

4.1.2 Xanthan Solution

The shear stress of ten different concentrations ranging from 100 to 10000 ppm of Xanthan solution as a function of shear rate from rotational testing is presented in Figure 4.3. Due to very low viscosities and resulting erratic measurements at low shear rates for solutions with a small concentration of Xanthan (100, 200, 500, 800 and 1000 ppm), results from ~0.5 to ~16 1/s are discarded in analyzing and interpretation. The relationship between shear stress and shear rate is not completely linear for the low concentrations, suggesting a shear-thinning effect. The low viscosities are in the range between 10^{-3} and 10^{-2} Pa·s (see Appendix A.1). From the figure, it is evident that there is little to no yield stress for low concentrations.

For solutions with higher concentrations of Xanthan (3000, 5000, 6000, 8000 and 10000 ppm) the linear relationship between shear stress and shear rate is less pronounced, and the shear-thinning effect is increasingly present. It also appears to be yield stress before shear onset at 0.5 1/s that increases with increasing viscosities and concentrations in the high concentration range. The viscosity (μ) of the higher concentrations of Xanthan as a function of shear rate is shown in Figure 4.4. The initial viscosity of 3000 ppm solution is ~4.7 Pa·s and increase towards ~26.9 Pa·s for the 10000 ppm solution. Due to shear-thinning, the viscosities drop to the 10^{-2}-10^{-1} Pa·s range for all solutions as the shear rate increases to 100 1/s. Table 4.2 shows the power and consistency index from curve fitting of the power law (Equation 2.2). The power index is lower than unity for all concentrations and generally decreasing with increasing concentration. The shear-thinning effect also increases with increasing concentration, accordingly. The consistency index increase with increasing concentration.

Table 4.2: Power index and consistency index from curve fitting of the power law (Equation 2.2) for ten different concentrations of Xanthan solution.

Conc. (ppm)	100	200	500	800	1000	3000	5000	6000	8000	10000
n (-)	0.82	0.74	0.55	0.47	0.44	0.18	0.13	0.10	0.10	0.12
κ (Pa·s^n)	0.0064	0.013	0.082	0.16	0.20	2.93	6.42	8.29	11.84	16.02

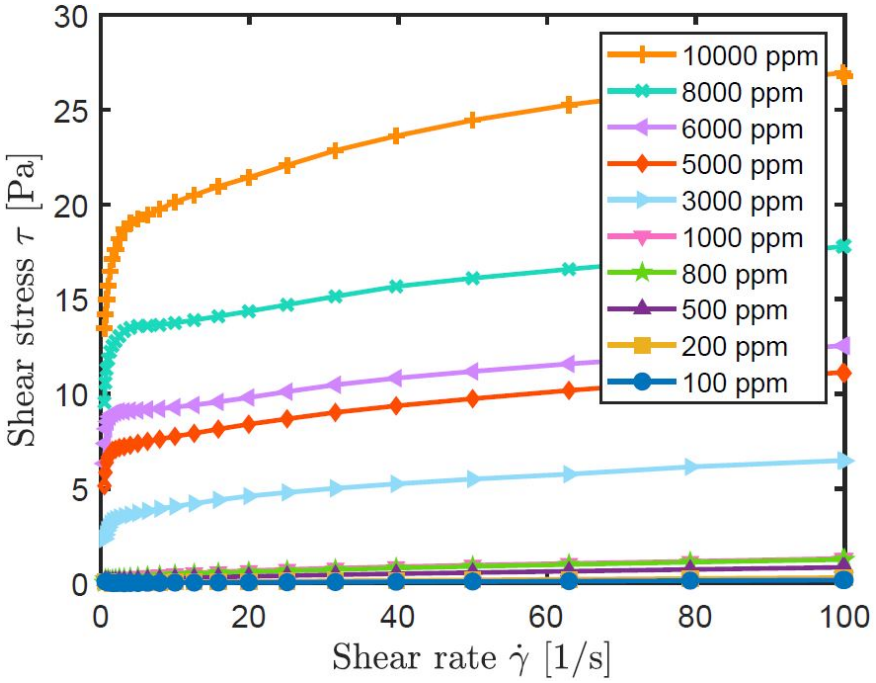

Figure 4.3: Shear stress of ten different concentrations of Xanthan solution as a function of shear rate (100 ppm (•), 200 ppm (■), 500 ppm (▲) and 800 ppm (★), 1000 ppm (▼), 3000 ppm (►), 5000 ppm (♦), 6000 ppm (◄), 8000 ppm (×) and 10000 ppm (+)).

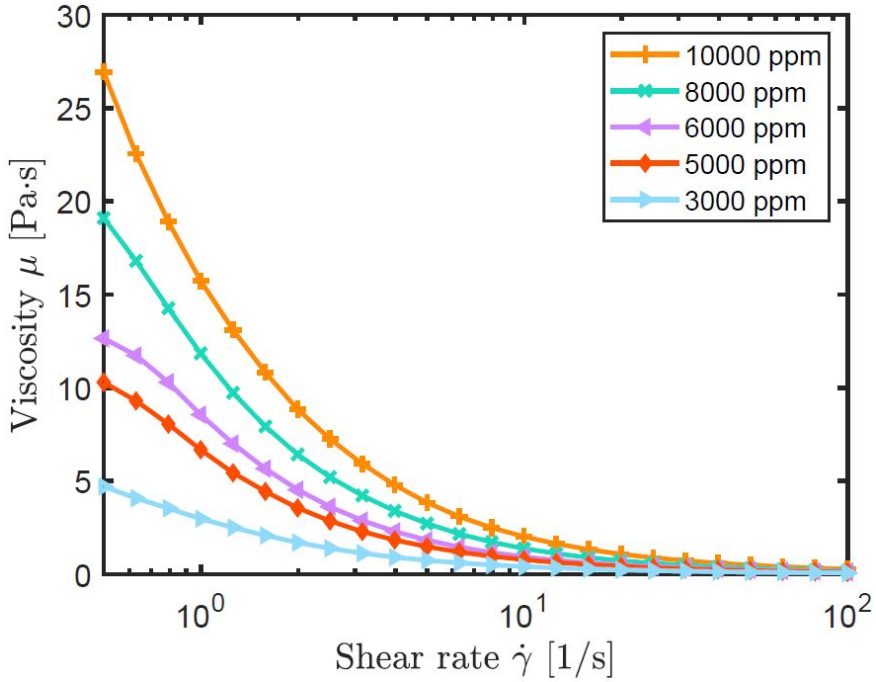

Figure 4.4: Viscosity of five different concentrations of Xanthan solution as a function of shear rate (3000 ppm (►), 5000 ppm (♦), 6000 ppm (◄), 8000 ppm (×) and 10000 ppm (+).)

The set strain amplitude (γ_0) for oscillation testing of Xanthan solution was not known prior to testing. An amplitude sweep was therefore performed on the sample with the highest concentration of Xanthan (10000 ppm) at a set angular frequency (ω) of 1 rad/s. Figure 4.5 shows the storage (elastic) modulus (G') and the loss (viscous) modulus (G") as a function of strain amplitude. The storage modulus has a linear profile up to a strain amplitude of approximately 15 % and a decreasing pattern above that value. The loss modulus has a linear behavior up to approximately 30 % and an increasing pattern above that value. A strain amplitude of 28 % was used in the following oscillation testing.

Figure 4.6 shows the storage modulus of Xanthan solution as a function of angular frequency. The storage modulus is similar for all the lower concentrations in the 100-1000 ppm range of Xanthan solution and has an increase with increasing angular frequency above ~10 rad/s. For the higher concentrations in the 3000-10000 ppm range of Xanthan solution, the storage modulus increases with both increasing concentration and increasing angular frequency.

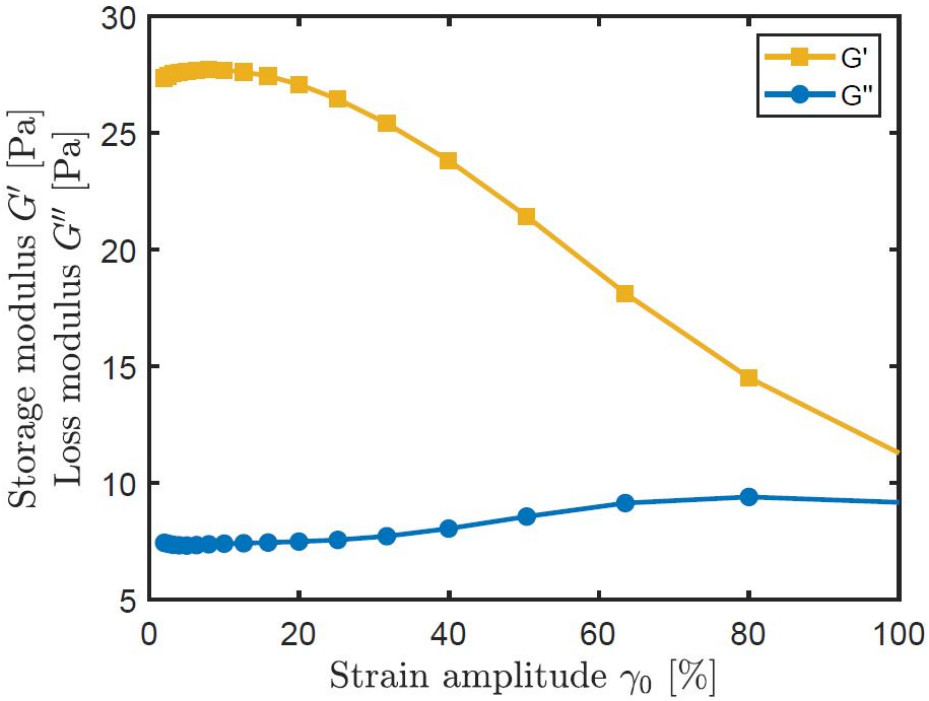

Figure 4.5: Storage modulus (■) and loss modulus (●) of 10000 ppm Xanthan solution as a function of strain amplitude at angular frequency = 1 rad/s.

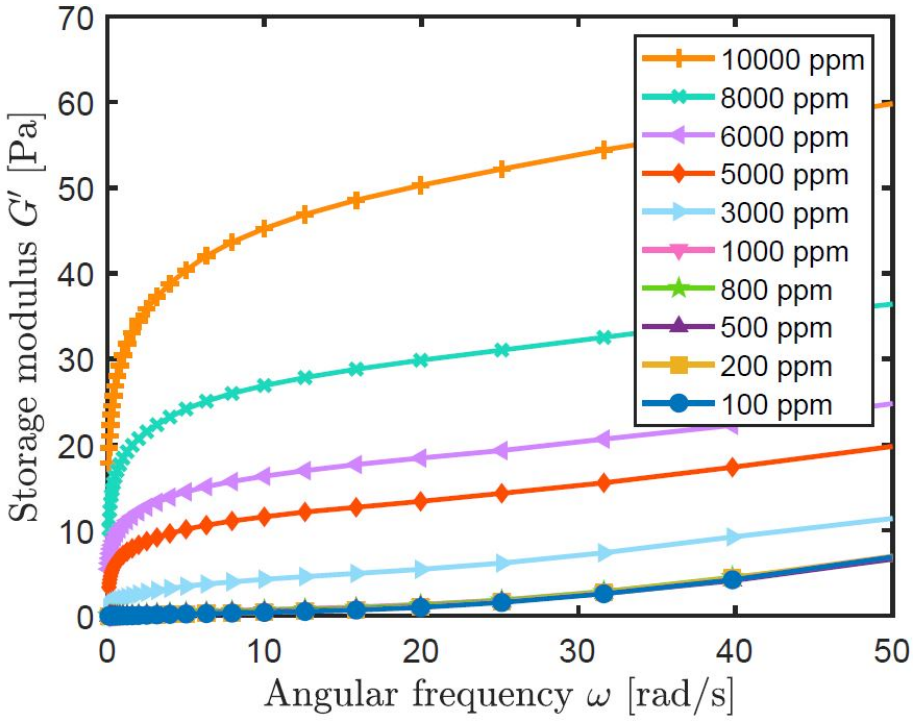

Figure 4.6: Storage modulus of ten different concentrations of Xanthan solution as a function of angular frequency (100 ppm (•), 200 ppm (■), 500 ppm (▲) and 800 ppm (★), 1000 ppm (▼), 3000 ppm (►), 5000 ppm (♦), 6000 ppm (◄), 8000 ppm (×) and 10000 ppm (+)).

Figure 4.7 shows the loss modulus as a function of angular frequency. The loss modulus is similar for the lower concentrations, but does not have the increasing behavior with increasing angular frequency as with the storage modulus and stays close to zero. For the higher concentrations, the loss modulus increases with both increasing concentration and increasing angular frequency. The loss modulus is however generally lower than the storage modulus for all concentrations and over the entire angular frequency range.

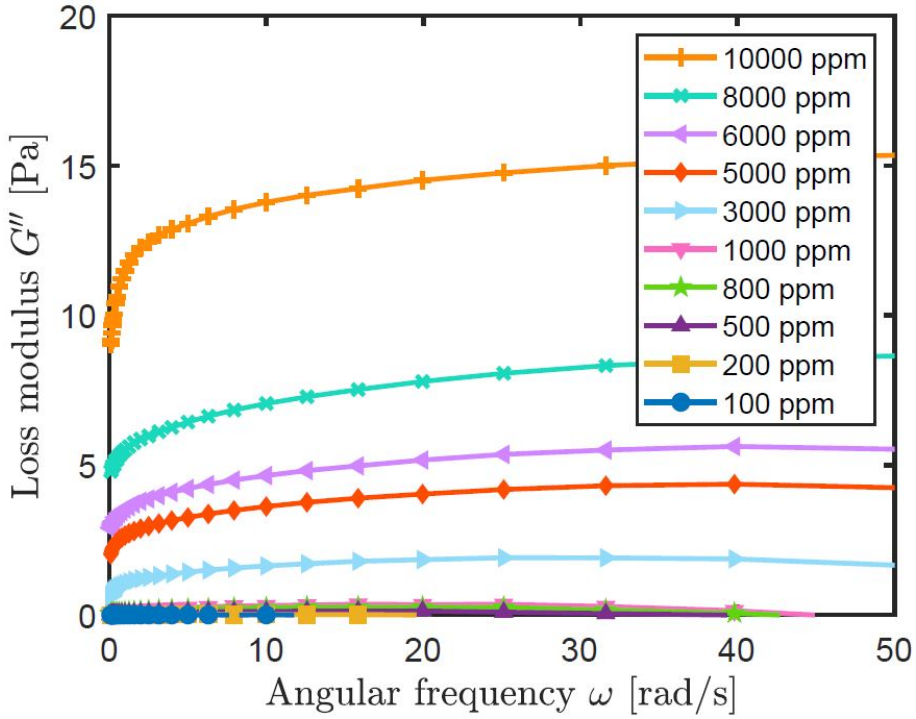

Figure 4.7: Loss modulus of ten different concentrations of Xanthan solution as a function of angular frequency (100 ppm (●), 200 ppm (■), 500 ppm (▲) and 800 ppm (★), 1000 ppm (▼), 3000 ppm (►), 5000 ppm (♦), 6000 ppm (◄), 8000 ppm (×) and 10000 ppm (+)).

4.1.3 Carbopol Gel

The shear stress of four different concentrations of Carbopol gel, two concentrations in a low range (0.2 % and 0.3 %) and two in a high range (1.6 % and 2.5 %), as a function of shear rate from rotational testing, is presented in Figure 4.8. There is significant shear-thinning behavior in both the high Carbopol gel concentrations. The low concentrations have some deviation from linear behavior but much less than for the high concentrations. There is little to no yield stress for the low concentrations. The high concentrations appear to have a yield stress of approximately 20 Pa for the 1.6 % sample and 60 Pa for the 2.5 % sample. The measured viscosities of the low concentrations are similar and remain in the 10^{-3} Pa·s range (see Appendix A.2). Figure 4.9 shows the viscosity of the high concentrations as a function of shear rate. The initial viscosity of the 1.6 % sample is ~44 Pa·s and ~129 Pa·s for the 2.5 % sample, both decreasing rapidly towards the 10^{-1} Pa·s

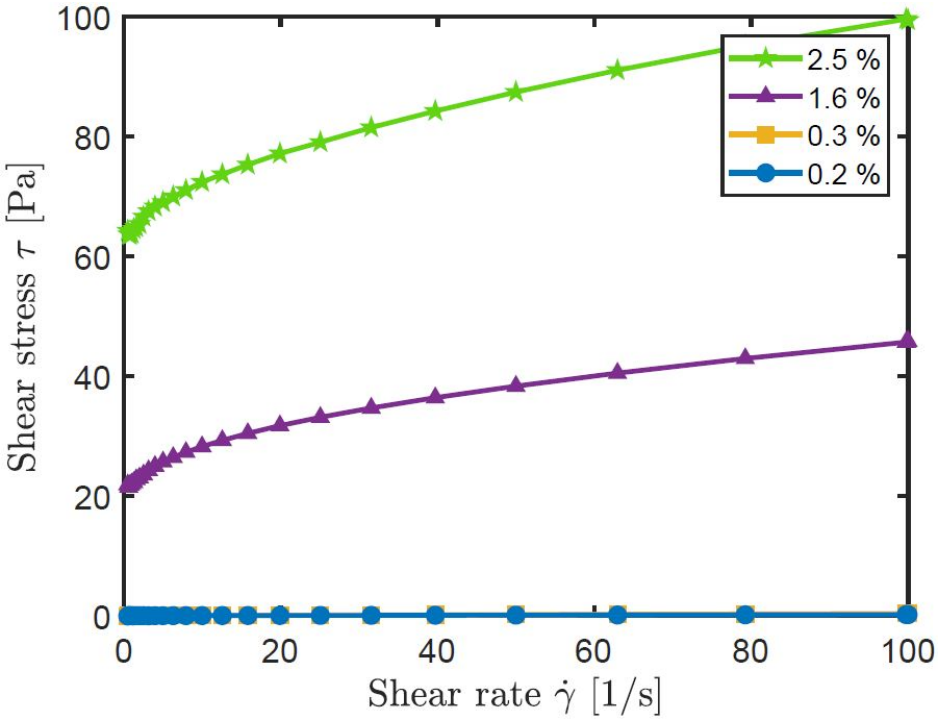

Figure 4.8: Shear stress of four different concentrations of Carbopol gel as a function of shear rate (0.2 % (●), 0.3 % (■), 1.6 % (▲) and 2.5 % (★)).

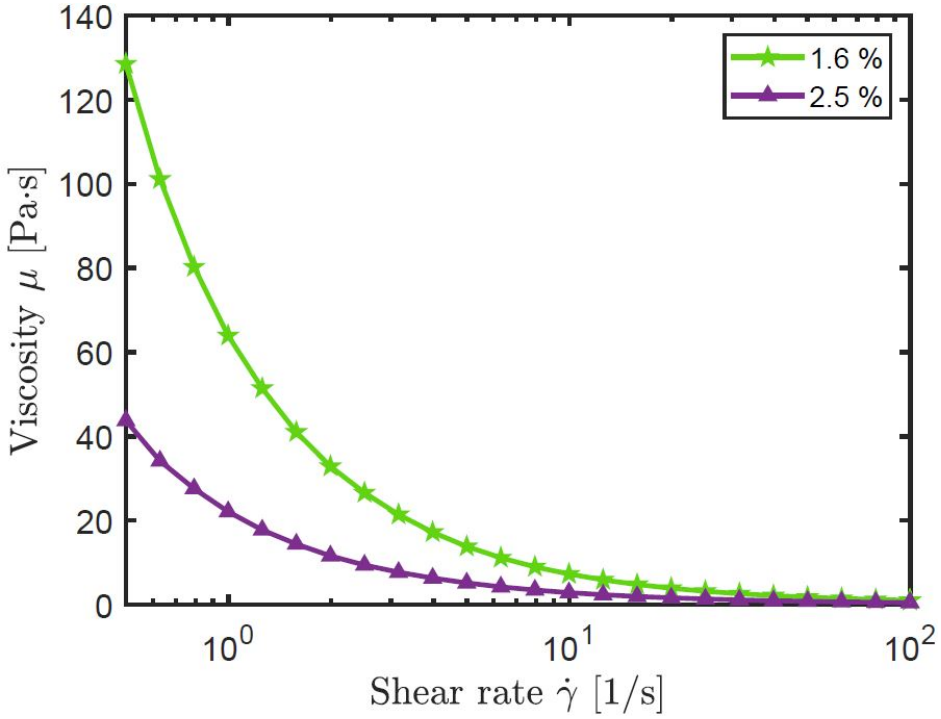

Figure 4.9: Viscosity of two high concentrations of Carbopol gel as a function of shear rate (1.6 % (▲) and 2.5 % (★)).

range with increasing shear rate due to shear-thinning. Table 4.3 shows the power index and consistency index from curve fitting of the power law (Equation 2.2). Due to the low viscosities of the low concentrations and resulting erratic measurements at low shear rates, the results from ~0.5 to ~6.3 rad/s are discarded in analyzing and interpretation. The power index of 0.2 % Carbopol is close but slightly lower than unity. When the concentration increases to 0.3 % Carbopol, the power index decreases dramatically to 0.91. The power index is very low at 0.17 and 0.10 for 1.6 % and 2.5 % Carbopol, respectively. The consistency index for the low concentrations are in the 10^{-3} Pa·s range and increase significantly to 21.64 and 63.87 for 1.6 % and 2.5 % Carbopol, respectively.

The strain amplitude of the oscillation testing of Carbopol gel was set to 1 %. Figure 4.10 shows the storage modulus of Carbopol gel as a function of angular frequency. The storage modulus of both lower concentrations remains close to zero before it starts to increase with an increasing angular frequency above ~10 rad/s. The 0.2 % Carbopol reaches a maximum of ~15 Pa at 100 rad/s while the 0.3 % Carbopol have a more rapid increase, reaching ~95 Pa at 100 rad/s. Initial storage modulus for 1.6 % and 2.5 % Carbopol are ~112 Pa and ~398 Pa, increasing towards ~240 Pa and ~472 Pa at 100 rad/s, respectively.

Figure 4.11 shows the loss modulus of Carbopol gel as a function of angular frequency. The loss modulus for the lowest concentrations is closely above zero for some low angular frequencies. The 1.6 % Carbopol has a positive loss modulus below approximately 67 rad/s and stay positive for the full angular frequency range for the 2.5 % Carbopol. However, the loss modulus of the 2.5 % Carbopol appears to be approaching zero with an angular frequency above 100 rad/s. The values are fluctuating at low frequencies, especially for

Table 4.3: Power index and consistency index from curve fitting of the power law (Equation 2.2) for four different concentrations of Carbopol gel.

Conc. (%)	0.2	0.3	1.6	2.5
n (-)	0.99	0.91	0.17	0.10
κ (Pa·s^n)	0.002	0.006	21.64	63.87

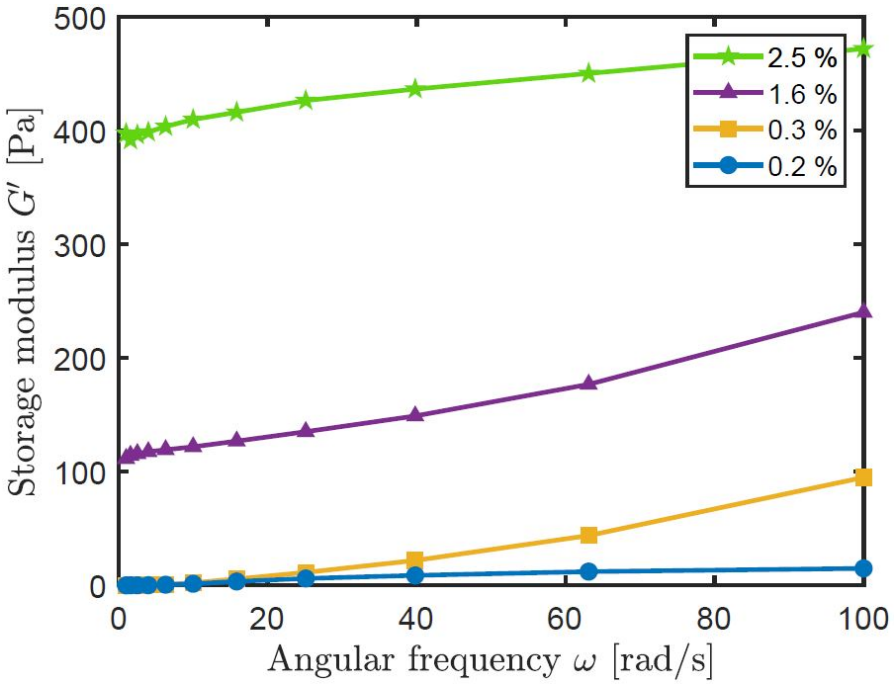

Figure 4.10: Storage modulus of four different concentrations of Carbopol gel as a function of angular frequency at 1 % strain amplitude (0.2 % (●), 0.3 % (■), 1.6 % (▲) and 2.5 % (★)).

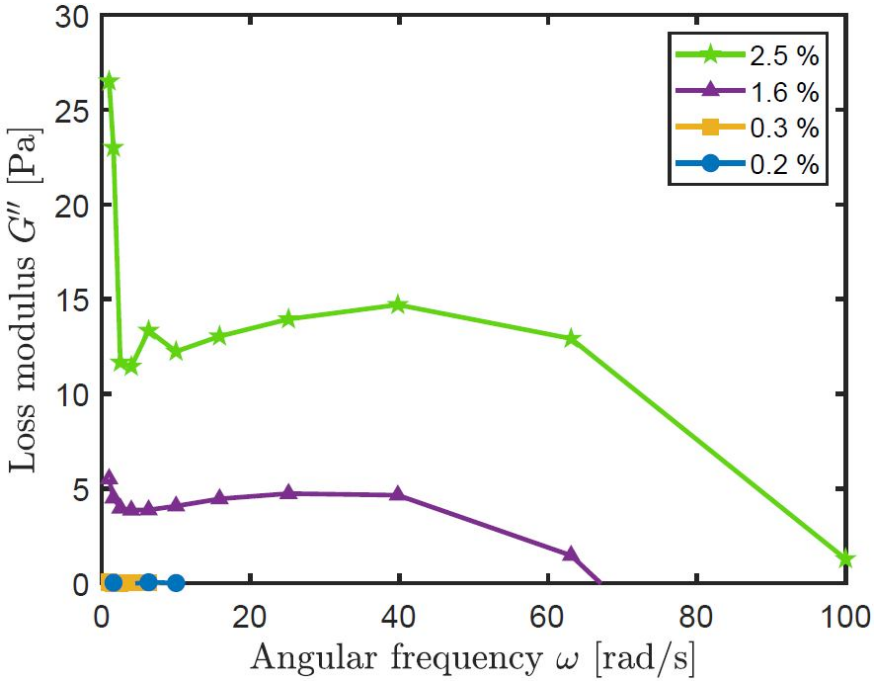

Figure 4.11: Loss modulus of four different concentrations of Carbopol gel as a function of angular frequency at 1 % strain amplitude (0.2 % (●), 0.3 % (■), 1.6 % (▲) and 2.5 % (★)).

the 2.5 % Carbopol. The loss modulus for the 1.6 % and 2.5 % Carbopol at 40 rad/s are ~4.65 Pa and ~14.70 Pa, respectively.

4.1.4 Polyethylene Oxide (PEO) Solution

The shear stress of five different concentrations of Polyethylene Oxide (PEO) solution as a function of shear rate from rotational testing is presented in Figure 4.12. There is some shear-thinning behavior at the lowest concentration of 3 %. The shear-thinning behavior increases with increasing concentration. Yield stress appears to be present for all concentrations as the shear stress at 0.5 1/s and increase with increasing PEO concentration from ~0.28 Pa for the 0.3 % solution up to ~27.7 Pa for the 7 % solution. Figure 4.13 shows the viscosity of the five different concentrations of PEO solution as a function of shear rate. The initial viscosities of the four lowest concentrations increase from ~0.55 Pa·s to ~17.6 Pa·s before it has a significant increase to ~55.5 Pa·s for the 7.4 % solution. The viscosities of the 7.4 % drop to ~6.3 Pa·s at 100 1/s and the viscosities of the lower concentrations at 100 1/s decreases

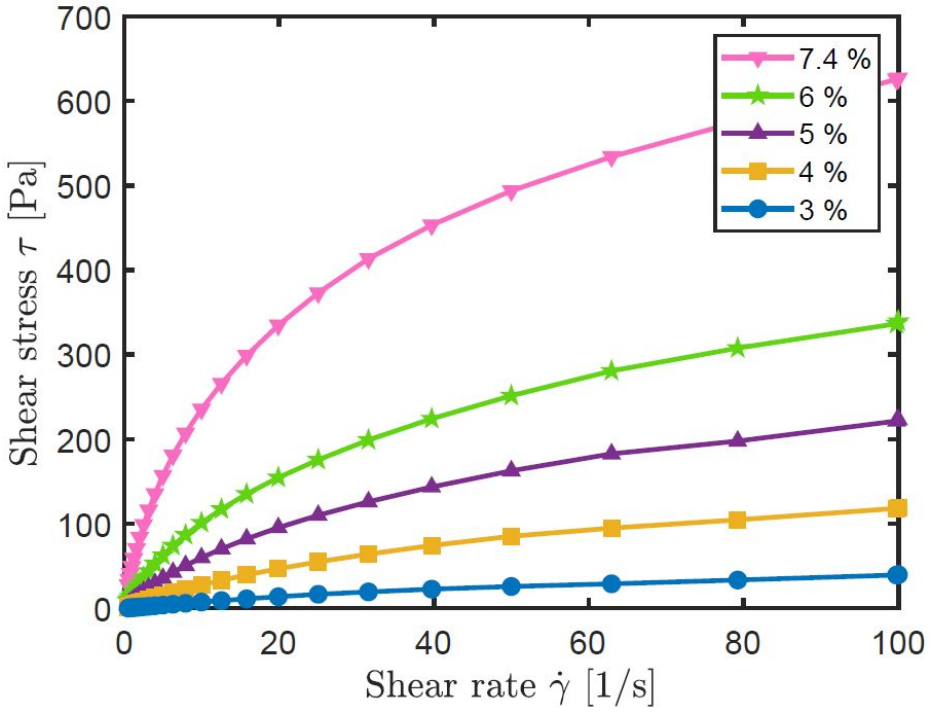

Figure 4.12: Shear stress of five different concentrations of PEO solution as a function of shear rate (3 % (●), 4 % (■), 5 % (▲), 6 % (★) and 7.4 % (▼)).

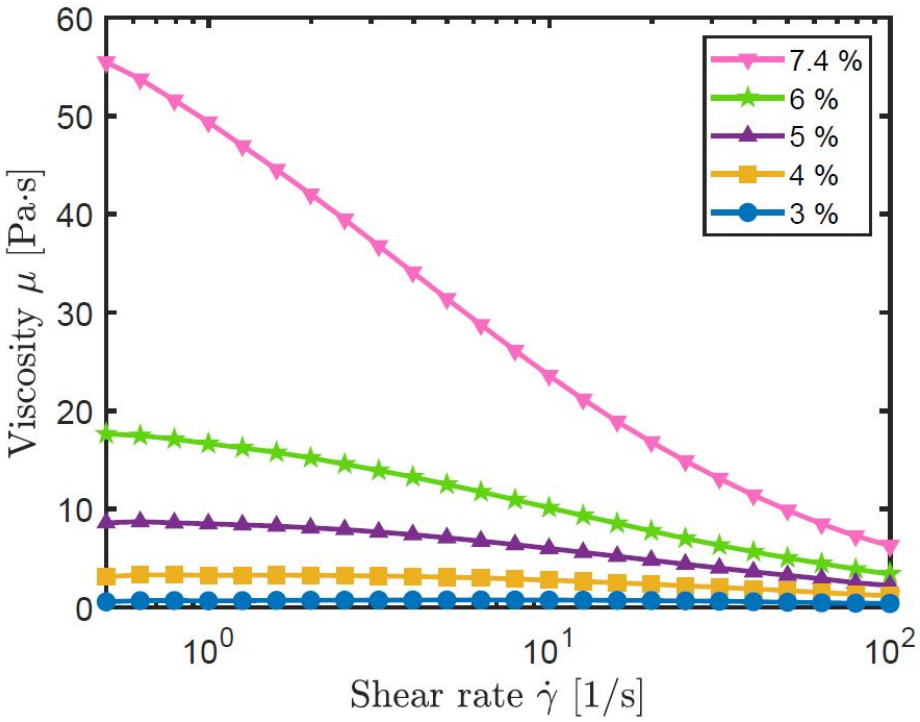

Figure 4.13: Viscosity of five different concentrations of PEO solution as a function of shear rate (3 % (●), 4 % (■), 5 % (▲), 6 % (★) and 7.4 % (▼)).

with decreasing concentration towards ~0.40 Pa·s for the 0.3 % solution. Table 4.4 shows the power index and consistency index from curve fitting of the power law (Equation 2.2). All power indices are lower than unity and decrease with increasing concentration of PEO, from 0.75 for the 3 % solution to 0.50 for the 7.4 % solution. The consistency indices are increasing with increasing concentration from 1.75 for the 3 % solution to 85.51 for the 7.4 % solution.

The set strain amplitude for oscillation testing of PEO solution was not known prior to testing. An amplitude sweep was performed on the 7.4 % solution at a set angular frequency of 1 rad/s. Figure 4.14 shows the storage

Table 4.4: Power index and consistency index from curve fitting of the power law (Equation 2.2) for five different concentrations of PEO solution.

Conc. (%)	3	4	5	6	7.4
n (-)	0.75	0.67	0.62	0.58	0.50
κ (Pa·s^n)	1.75	7.56	17.49	31.22	85.51

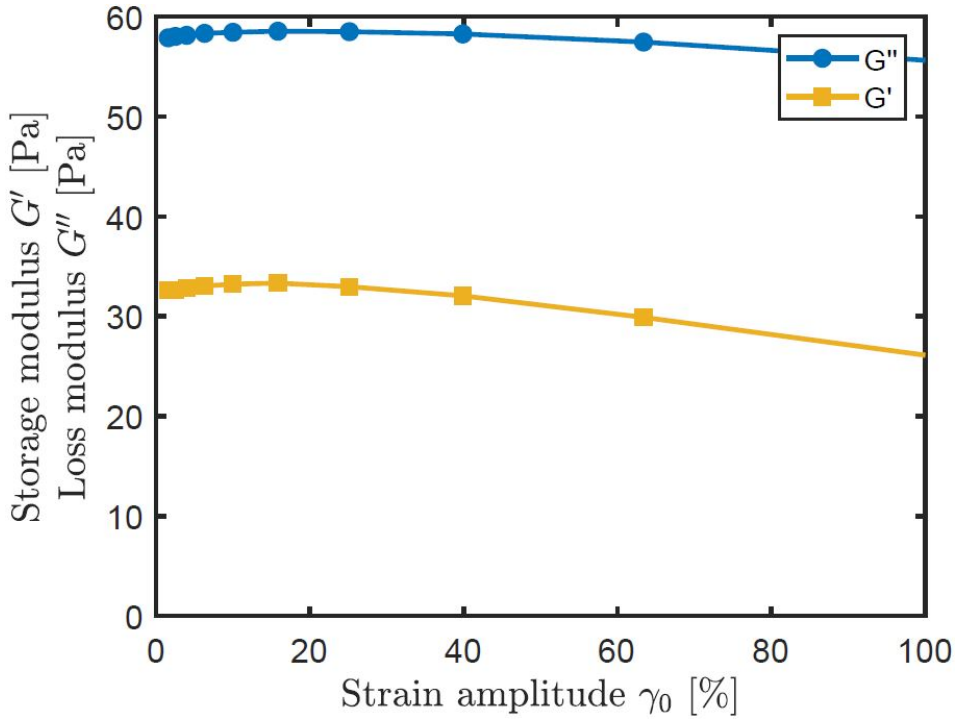

Figure 4.14: Storage modulus (■) and loss modulus (●) of 7.4 % PEO solution as a function of strain amplitude at angular frequency = 1 rad/s.

and loss modulus as a function of strain amplitude. The storage modulus has a linear pattern up to approximately 15 % strain amplitude and a slightly decreasing behavior above that value. The loss modulus behaves linearly up to approximately 40 % strain amplitude and has similar decreasing behavior to the storage modulus above that value. The strain amplitude was set to 15 % in the following oscillation tests.

Figure 4.15 shows the storage modulus of PEO solution as a function of angular frequency. The initial storage modulus values at 0.5 rad/s start at ~0.012 Pa for the 3 % solution and increase with increasing concentration up to ~9.58 Pa for the 7.4 % solution. All concentrations have increased storage modulus with increasing angular frequency with a maximum, increasing with increasing concentration from ~33.87 Pa for the 3 % solution to ~555.28 Pa for the 7.4 % solution at 100 rad/s.

The loss modulus of PEO solution as a function of angular frequency is shown in Figure 4.16. The loss modulus is generally lower than the storage modulus for all concentrations. The initial values of the loss modulus at

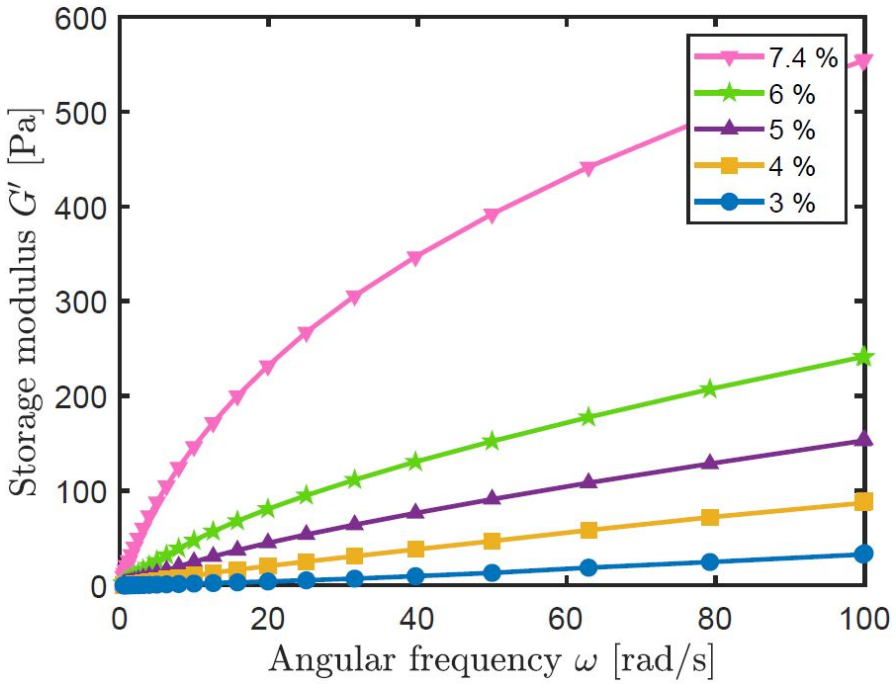

Figure 4.15: Storage modulus of five different concentrations of PEO solution as a function of angular frequency at 15 % strain amplitude (3 % (●), 4 % (■), 5 % (▲), 6 % (★) and 7.4 % (▼)).

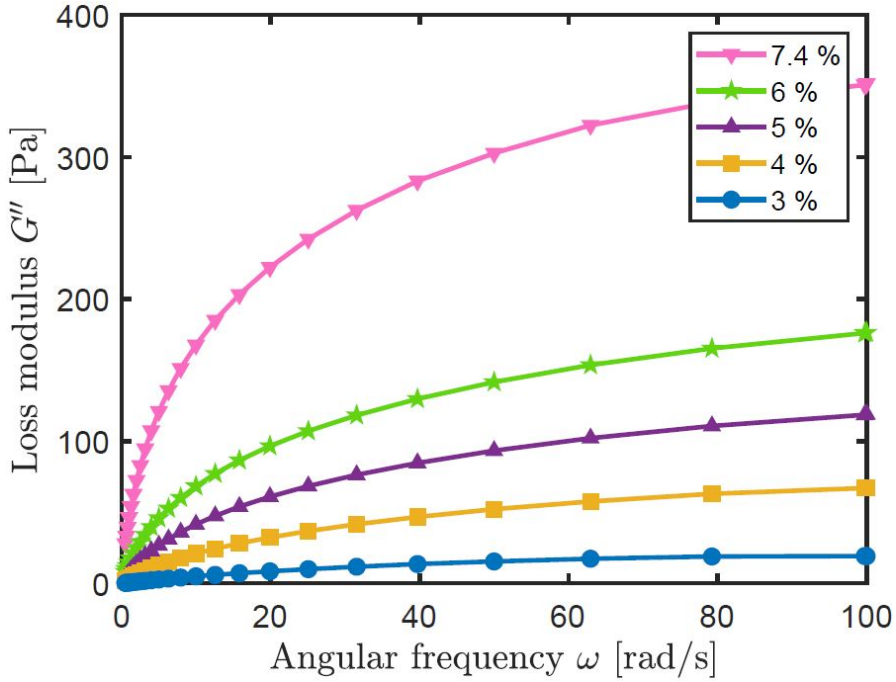

Figure 4.16: Loss modulus of five different concentrations of PEO solution as a function of angular frequency at 15 % strain amplitude (3 % (●), 4 % (■), 5 % (▲), 6 % (★) and 7.4 % (▼)).

0.5 rad/s are ~0.30 Pa for the 3 % solution and increasing with increasing concentrations towards ~28.0 Pa for the 7.4 % solution. All concentrations have increasing loss modulus with increasing angular frequency. The maximum values at 100 rad/s range with increasing concentration from ~19.15 Pa for the 3 % solution to ~351.71 Pa for the 7.4 % solution.

Chapter 5

Discussion

5.1 Fluid Models

5.1.1 Silicone Oil and Coke Particles

Figure 4.1 shows the shear stress (τ) as a function of shear rate ($\dot{\gamma}$) for silicone oil and silicone oil with coke particles. When compared to the shear stress of pitch and binder matrix from Figure 2.8 it can be seen that the shear stress of silicone oil is similar to the shear stress of pitch at 178 °C, which is the industrial processing temperature. The shear stress of silicone oil and pitch are approximately 250 Pa at 100 1/s. When fine coke particles are added, the shear stress increases with increasing particle concentration for both fluids, but more rapidly for the pitch system. At 15 % particles, the shear stress is approximately 500 Pa for the binder matrix and 300 Pa for the silicone oil system at 100 1/s. Addition of fine coke particles in the range 5 to 15 % therefore have a more significant impact on the shear stress for pitch and binder matrix than for silicone oil at 178 °C up to 100 1/s. The shear stress of pitch and binder matrix at 166 °C is much higher ranging from ~700 Pa for pitch to ~1300 Pa for binder matrix with 15 % particles than the shear stress of the silicone oil system. At 190 °C, the shear stress of pitch and binder matrix is lower with approximately 250 Pa as the maximum for 15 % particles.

The power and consistency index of silicone oil and silicone oil with coke particles are shown in Table 4.1. The power index is equal to unity for all samples, demonstrating a nearly Newtonian behavior in the shear rate range 0 to 100 1/s. Pitch have a power index of unity at all temperatures, which decreases with increasing concentration of added coke particles in the shear rate range 0 to 200 1/s. This can be seen in Table 2.4 showing power index and consistency index of pitch and binder matrix at 166 °C, 178 °C and 190 °C. As the power index of pitch and binder matrix is derived from a higher shear rate range, it is possible that it would be closer to unity if derived from the same shear rate range as the silicone oil system. Regardless, binder matrix with 5 to 15 % coke particles have an obvious shear-thinning behavior at all temperatures. The consistency index of silicone oil and pitch at 178 °C is 2.75 Pa·s^n and 2.55 Pa·s^n, respectively. When coke particles are added to silicone oil, the consistency index increases with increasing concentration up to 3.05 Pa·s^n for the 15 % sample, which is much lower than that of 6.99 Pa·s^n for the 15 % binder matrix. The consistency index of pitch and binder matrix at 166 °is much higher with the minimum of 7.27 Pa·s^n for pitch. At 190 °C, the consistency index is more similar to the silicone oil system ranging from 1.31 Pa·s^n to 3.51 Pa·s^n compared to 2.75 Pa·s^n to 3.05 Pa·s^n.

Pure silicone oil may be used as a fluid model for pitch at 178 °C as the shear stress, power index and consistency index are similar. No apparent yield stress was detected in the silicone oil samples as with pitch and binder matrix. The transparency of silicone oil can also be utilized for visualization of particle movement. Silicone oil with coke particles had a similar consistency index as the binder matrix at 190 °C, but the other rheological properties did not coincide with that of binder matrix at any temperature.

5.1.2 Xanthan Solution

The shear stress as a function of shear rate of ten different concentrations of Xanthan solution is shown in Figure 4.3. Compared to the shear stress of pitch and binder matrix at all temperatures, the shear stress is much lower for all concentrations of Xanthan solution at 100 1/s. The highest shear stress

is just above 25 Pa for 10000 ppm Xanthan solution, and the lowest shear stress is approximately 100 Pa for pitch at 190 °C, which increases with increasing additions of coke particles and decreasing temperature. It can be expected that the shear stress of binder matrix with increasing fine coke particles up to 60 wt. % would continue to increase based on the results up to 35 wt. %. Xanthan solution of concentrations ranging from 3000 to 10000 ppm also have an apparent yield stress, which is not detected in any of the pitch and binder matrix measurements.

Table 4.2 shows the power and consistency index of Xanthan solution. The shear-thinning behavior is very pronounced at the lowest concentration of 100 ppm with a power index of 0.82 and increases to a power index of 0.12 for 10000 ppm. The lowest power index found for pitch and binder matrix was 0.87 for 35 wt. % at 166 °C. Even if the power index can be expected to drop with increasing coke particle content up to 60 wt. %, the range of the power index for Xanthan solution is much lower than the existing values. The consistency index for the low range of Xanthan solution (100-1000 ppm) are all below zero. It increases from 2.93 Pa·s^n for 3000 ppm to 16.02 Pa·s^n for 10000 ppm and is comparable to the consistency index of pitch and binder matrix. However, the associated power index at the same concentration is much lower than what is the case for pitch and binder matrix.

The storage modulus (G′) and loss modulus (G″) of Xanthan solution as a function of angular frequency (ω) are shown in Figure 4.6 and Figure 4.7, respectively. When comparing to the storage modulus and loss modulus for pitch and binder matrix (Figure 2.9 and Figure 2.10, respectively), it is evident that both elastic and viscous properties of Xanthan solution are much lower than that of pitch and binder matrix at all concentration of coke particles and temperatures. The storage modulus of Xanthan solution is also higher than the loss modulus for Xanthan solution, while the opposite is true for pitch and binder matrix. As can be seen from Figure 4.5, the constant plateau of the storage modulus indicating the linear viscoelastic region is up to approximately 15 %. The strain amplitude (γ_0) used for the following oscillation tests was set to 28 % based on the constant plateau of the loss modulus up to approximately 30 %. The results from the oscillation tests of

Xanthan solution may therefore be invalid due to the possible irreversible change or even destruction of the structure related to strain amplitudes exceeding the linear viscoelastic region [78].

None of the concentrations of Xanthan solution had overall similar rheological properties as pitch and binder matrix in the reviewed concentration range. Xanthan solution has a semi-transparent nature, but the order of property discrepancy is too great. The shear stress, power index, consistency index, elastic modulus and viscous modulus of Xanthan solution was much lower than that of pitch and binder matrix for the entire concentration range in addition to the presence of an apparent yield stress.

5.1.3 Carbopol Gel

Figure 4.8 shows shear stress as a function of shear rate for four different concentrations of Carbopol gel. The shear stress of the two lowest concentrations (0.2 % and 0.3 %) is very low while it is slightly higher for the two highest concentrations (1.6 % and 2.5 %). However, when comparing to the shear stress of pitch and binder matrix at all concentrations of coke particles and temperatures, the shear rate of the highest concentrations of Carbopol gel is much lower in the shear rate range from 0.5 to 100 1/s. An apparent yield stress was also detected for the two highest concentrations of Carbopol gel, which is not present for pitch and binder matrix.

The power index of the 0.2 % and the 0.3 % samples from Table 4.3 are similar to some of the pitch and binder matrix power indices, indicating a shear-thinning behavior. The consistency index is still as low as 0.002 and 0.006, which is much lower than that of binder matrix in the same power index range. For 1.6 % and 2.5 % samples, the consistency index is higher with 21.64 $Pa{\cdot}s^n$ and 63.87 $Pa{\cdot}s^n$, which is close to the consistency index of binder matrix at 166 °C with 20-35 wt. % coke particles. The power index is however 0.17 and 0.10, and much lower than that of 0.90 to 0.87 of binder matrix from 20 to 35 wt. % coke particles.

Storage modulus as a function of angular frequency of Carbopol gel is shown in Figure 4.10. The Carbopol samples with a concentration of 0.2 % and

0.3 % both have an initial storage modulus close to zero. The initial storage modulus of pitch and binder matrix is also close to zero for almost all concentrations of coke particles and temperatures. The 0.2 % Carbopol sample has a lower increase with increasing angular frequency towards 100 rad/s than pitch and binder matrix. The 0.3 % Carbopol increases to almost 100 Pa at 100 rad/s, which is close to the value of binder matrix with high concentrations of coke particles up to 60 wt. % at all temperatures. For the 1.6 % and 2.5 % Carbopol samples, the initial storage modulus is ~100 Pa and ~400 Pa, respectively, and much higher than that of pitch and binder matrix. At 100 rad/s the storage modulus is higher than all pitch and binder matrix at all temperatures, except for the binder matrix with 60 wt. % coke particles at 166 °C. The loss modulus as a function of angular frequency of Carbopol gel is shown in Figure 4.11 and it is evident that the results are erroneous as the loss modulus is negative or approaches negative values with increasing angular frequency for all concentrations. Possible explanations include the use of strain amplitude exceeding the linear viscoelastic region and a resulting structure alteration or destruction, thus producing incorrect values. Due to the erroneous loss modulus, all results from the oscillation testing of Carbopol gel, including storage modulus, could also be incorrect.

Shear rate, power index, consistency index, and yield stress presence of Carbopol gel did not match those of pitch and binder matrix. Carbopol gel is semi-transparent with decreasing transparency with increasing concentration. The elastic properties (storage modulus) of Carbopol gel were somewhat similar to the elastic properties of pitch and binder matrix. However, the loss modulus values of Carbopol gel question the validity of the storage modulus values obtained and makes viscoelastic comparison to pitch and binder matrix difficult.

5.1.4 Polyethylene Oxide (PEO) Solution

Figure 4.12 shows the shear stress as a function of shear rate for five different concentrations of PEO solution. The shear stress of pitch and binder matrix at 166 °C reaches values from approximately 700 Pa for pitch to 2750 Pa

for binder matrix with 35 wt. % coke particles at 100 1/s. PEO solution of 7.4 % approaches a shear stress of ~650 Pa at 100 1/s. This is the highest value, which is even lower than the lowest shear stress value measured at 166 °C for pitch and binder matrix. The 3 % solution has a shear stress of approximately 30 Pa at 100 1/s. At 178 °C, the shear stress at 100 1/s of pitch and binder matrix increase with increasing coke particle concentration from ~250 Pa (pitch) up to ~1200 Pa (35 wt. %), suggesting that the lower concentrations of coke particles have similar shear stress as the PEO solutions. The 35 wt. % binder matrix approaches ~700 Pa at 100 1/s as the highest at 190 °C, while pitch and binder matrix of lower concentration of fine coke particles have lower shear stress, thus remaining in the shear stress range of PEO solutions. There is a low apparent yield stress, increasing with increasing concentration of PEO.

The power and consistency index of PEO solution are shown in Table 4.4. All concentrations show shear-thinning behavior with the power index starting at 0.75 for 3 %, decreasing towards 0.50 for 7.4 %. Pitch and binder matrix up to 35 wt. % all have a higher power index at all temperatures, but if the trend of decreasing power index with increasing coke particle concentration continues, it is possible that the power index of the binder matrix highest concentrations of coke particles will be in the range of PEO solution power indices. The consistency index of PEO solution from 3 % to 6 % are all within the range of pitch and binder matrix at all temperatures, while the 7 % solution has a consistency index of 85.51 $Pa{\cdot}s^n$, exceeding the highest value of the 35 wt. % binder matrix at 166 °C with 66.66 $Pa{\cdot}s^n$. If it is also assumed that the consistency index will continue to increase for binder matrix with increasing coke particle concentration, the 7 % consistency index may also be in the range of the higher concentrations of coke particles.

Figure 4.15 shows the storage modulus as a function of angular frequency for five concentrations of PEO solution and Figure 5.1 shows the same data in a logarithmic scale next to the storage modulus of pitch and binder matrix at 178 °C to visualize the similarities of elastic behavior with concentration and angular frequency in the two systems. The storage modulus of PEO solutions increases more rapidly with increasing angular frequency but remains in

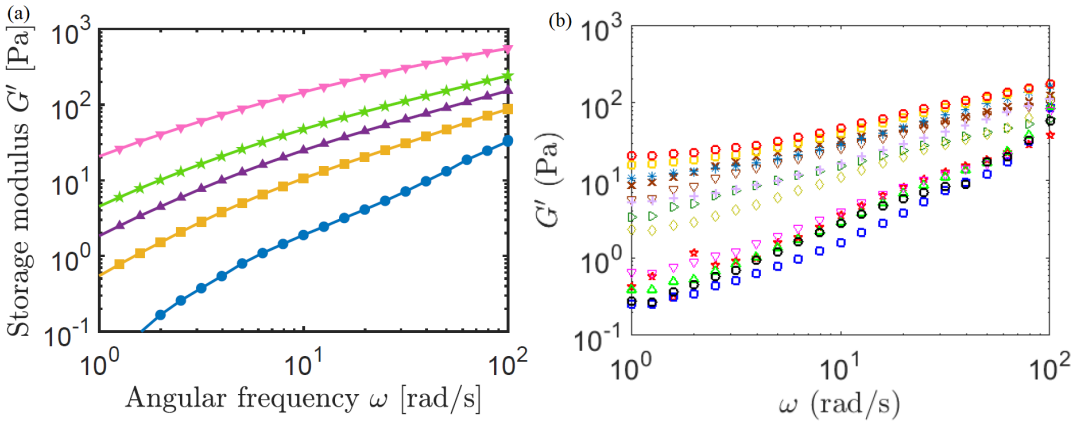

Figure 5.1: Storage modulus as a function of angular frequency of (a) five different concentrations of PEO solution at 15 % strain amplitude (3 % (●), 4 % (■), 5 % (▲), 6 % (★) and 7.4 % (▼)) and (b) pitch and binder matrix with concentrations from 0 wt. % to 60 wt. % fine coke particles.

the same range as the pitch and binder matrix with both higher and lower values. Pitch and binder matrix at 166 °C and 190 °C have a similar increase in storage modulus with angular frequency as pitch and binder matrix at 178 °C, but is generally higher at 166 °C and lower at 190 °C. The range of storage modulus of PEO solutions closely covers the entire range of pitch and binder matrix at all temperatures.

The loss modulus as a function of angular frequency of five concentrations of PEO solution is shown in Figure 4.16. Figure 5.2 shows the same data in a logarithmic scale next to the loss modulus of pitch and binder matrix at 178 °C to compare the viscous behavior of the two systems with concentration and angular frequency. In contrast to the storage modulus, the loss modulus increases more slowly with increasing angular frequency for the PEO solutions than for pitch and binder matrix. The initial loss modulus values are similar, but the loss modulus at 100 rad/s are generally much lower for PEO solution than for pitch and binder matrix. Loss modulus of pitch and binder matrix is even higher at 166 °C and has a consequently higher discrepancy with the loss modulus of PEO solutions. At 190 °C, the loss modulus of pitch and binder matrix is lower and therefore more similar to the PEO solutions.

Many rheological parameters of different concentrations of PEO solutions

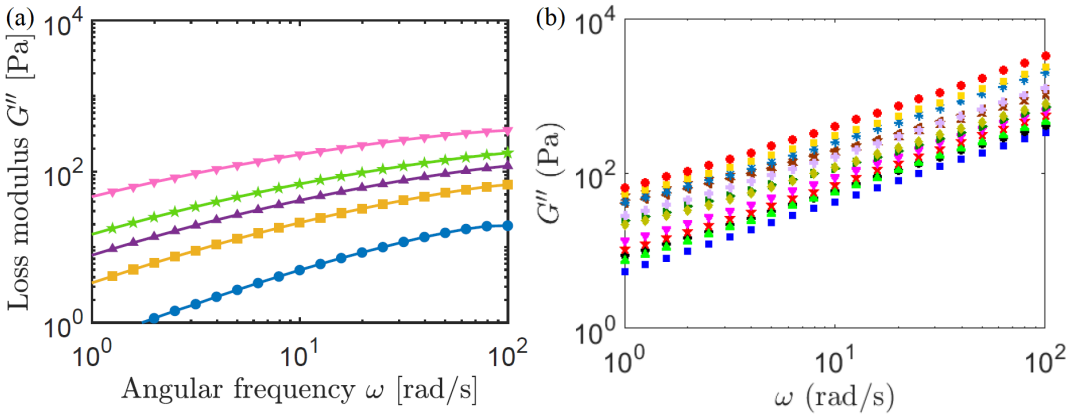

Figure 5.2: Loss modulus as a function of angular frequency of (a) five different concentrations of PEO solution at 15 % strain amplitude (3 % (●), 4 % (■), 5 % (▲), 6 % (★) and 7.4 % (▼)) and (b) pitch and binder matrix with concentrations from 0 wt. % to 60 wt. % fine coke particles.

are similar to those of pitch and binder matrix. The shear stress resemblance increase with increasing temperatures. The power index of PEO solutions are too low compared to the power index of pitch and binder matrix with coke particle concentration up to 35 wt. %, but can be accurate for higher concentrations of coke particles if the general trend of increased shear-thinning behavior with increasing particle concentration continues. Consistency indices were comparable to the existing pitch and binder matrix measurements, and the consistency index 7.4 % is likely comparable to binder matrix with increased particle concentration. The viscous component of pitch and binder matrix is generally higher than the elastic component at all temperatures and angular frequencies. The same is true for PEO solutions at low angular frequencies, while the elastic component surpasses the viscous component at increased angular frequencies as the storage modulus increases more rapidly than the loss modulus. The range of the storage modulus of PEO solutions nearly covers the storage modulus of pitch and binder matrix overall, and the loss modulus had similar initial values. At low temperatures and increased angular frequencies, the discrepancies between the loss modulus of PEO solutions and pitch and binder matrix increased. From Figure 4.14, it is evident that the linear viscoelastic region does not exceed 15 % strain amplitude, which was used in the oscillation testing. It can therefore be assumed that the results from the oscillation testing of PEO solution

are valid. PEO solution also has a semi-transparent nature and possibility of visual contrast between particles and fluid.

5.2 Suspension Models

Figure 5.3 shows the viscosity of pitch and binder matrix at 178 °C as a function of volume fraction from Mollaabbasi et al. [11] at high shear rate (100 1/s) and low shear rate (1 1/s) with different suspension models. As suspension models are based on volume fraction, weight fractions from 0 to 35 wt. % from measurements have been translated to volume fractions from 0 to ~25.5 %. The viscosity of pitch at 178 °C and a volume fraction of 0 is 2.54 Pa·s, independent of shear rate as pitch is a Newtonian fluid [11]. The blue lines represent modifications of Einstein's equation (Equation 2.5) with a second-order term to describe inter-particle interaction (Equation 2.6). Three different values of K have been used: 4.375 (●) [62, 63], 14.1 (◀) [64]

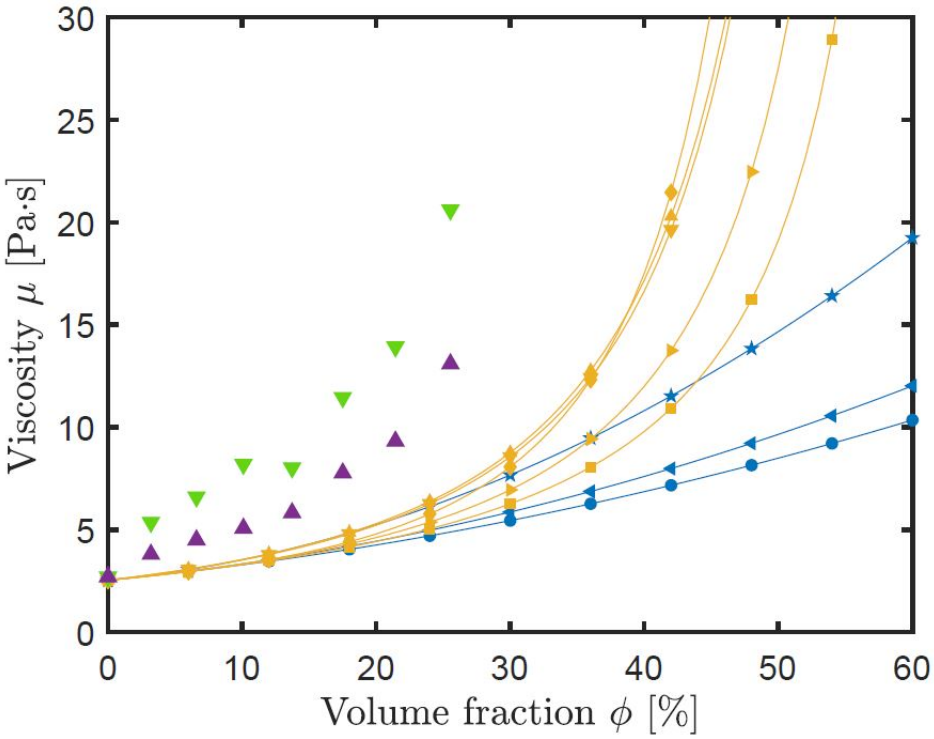

Figure 5.3: Viscosity of pitch and binder matrix as a function of concentration of fine particles at high shear rate = 100 1/s (▲) and low shear rate = 1 1/s (▼) at 178 °C and different suspension models.

and 6.2 (★) [65]. The yellow lines represent suspension models relating the influence particle concentration and maximum packing volume fraction on viscosity: Equation 2.7 (►) [66], Equation 2.8 (▲) [67], Equation 2.9 (▼) [68], Equation 2.10 (■) [69] and Equation 2.11 (♦) [70]. The maximum packing volume fraction used was 0.637 for random close packed arrangement [41].

None of the suspension models are able to predict the experimental results from both low and high shear rates at 178 °C. As the viscosity is lower at 190 °C, the experimental results are closer to those of suspension models, while the opposite is true for 166 °C [11]. The suspension models including a maximum packing volume fraction (yellow lines) are closer to experimental results than suspension models based on Einstein's equation. Zarraga et al. [70] with Equation 2.11 (♦) have the model nearest experimental results. The deviation of the experimental results from the suspension models increases with increasing volume fraction. Assuming that this trend continues above 35 wt. % up to 60 wt. % the suspension models will never coincide with the experimental results.

It is evident from comparing experimental results with selected suspension models that the viscosity of binder matrix depends on other parameters than only the volume fraction. In addition to shear rate and temperature, tendency of particles to agglomerate, particle size, particle size distribution, and deformation operation are among the properties that affect binder matrix viscosity to some extent [47]. Also, the maximum packing volume fraction decreases with decreasing particle size distribution. If the particle size distribution and consequently the maximum packing volume fraction is lower than assumed in calculations, the suspension models would be closer to the experimental results.

Chapter 6

Conclusion and Further Work

The purpose of this work was to investigate different fluid models that have similar rheological properties of pitch and binder matrix at room temperature. Silicone oil was the fluid model most similar to pitch at the industrial temperature, 178 °C. Additions of fine coke particles did not have the same effect as on pitch and binder matrix. Changing the added coke particles to transparent particles with different properties, the rheological properties may be tuned to coincide with binder matrix while retaining the optical transparency of silicone oil. Xanthan solution did not show similar rheological properties at any concentration as pitch and binder matrix. Only the elastic properties of Carbopol gel matched those of pitch and binder matrix. The validity of elastic and viscous modulus of both Xanthan solution and Carbopol gel was questioned due to the possibility of strain amplitudes exceeding the linear viscoelastic region. PEO solution had some similar rheological properties of pitch and binder matrix. The power index of PEO solution was too small compared to pitch and binder matrix with coke particle concentrations up to 35 wt. %. However, if the power index of binder matrix continues to decrease with increasing coke particle concentration up to 60 wt. %, PEO solution may be used as a fluid model for high concentration binder matrix if the other rheological properties remain close to those of

pitch and binder matrix. PEO solution also had optical semi-transparency. From comparing the viscosity of binder matrix with suspension models as a function of volume fraction, it is evident that other parameters than volume fraction contribute to the determination of rheological properties of binder matrix. Shear rate, temperature, maximum packing volume fraction, and other particle parameters are factors that should be considered.

Rotational testing of binder matrix with fine coke particle concentration exceeding 35 wt. % has not been done due to limitations of the used method [11]. A complete analysis of the rheological properties of binder matrix up to the industrial coke particle concentration of ~60 wt. % would contribute to the understanding of anode paste behavior during compaction and enable further development of fluid models. The rheological properties of a range of concentrations from 3 % to 7.4 % PEO solution have been determined but could be tuned more accurately if the rheological properties of the entire range of pitch and binder matrix were known. Furthermore, if PEO solution can be used as a fluid model for binder matrix, it may be possible to use a high-speed camera to track the movement of coarse coke particles in the PEO solution, depending on the level of optical transparency. If silicone oil with added transparent particles could have similar rheological properties as binder matrix, it could also be used as a fluid model to track coarse particle movement in.

Bibliography

[1] The International Aluminium Institute. Primary Aluminium Production. [cited 24.01.2019]. Available from http://www.world-aluminium.org/statistics/, 2019.

[2] Roger N. Lumley. *Fundamentals of aluminium metallurgy: Production, processing and applications*. Woodhead Publishing, 2010.

[3] Kai Grjotheim and Halvor Kvande. Introduction to Aluminium Electrolysis: Understanding the Hall-Héroult Process. 2nd edition, Düsseldorf, Aluminium-Verlag. 1993.

[4] Felix Keller and Peter O. Sulger. Preconditions for the Production of High Quality Anodes. In *Anode Baking: Baking of Anodes for the Aluminium Industry*, pages 17–60. R&D Carbon Limited, Sierre, Switzerland, 2nd edition, 2008.

[5] Trond Brandvik, Zhaohui Wang, Arne Petter Ratvik, and Tor Grande. Autopsy of Refractory Lining in Anode Kilns with Open and Closed Design. *International Journal of Applied Ceramic Technology*, pages 1–12, 2018.

[6] Kristine Louise Hulse. The Role and Behaviour of Anodes in the Cell. In *Anode Manufacture: Raw materials, Formulation and Processing Parameters*, chapter 1, pages 1–20. R&D Carbon Limited, Sierre, Switzerland, 1st edition, 2000.

[7] Kamran Azari, Houshang Alamdari, Gholamreza Aryanpour, Donald Ziegler, Donald Picard, and Mario Fafard. Compaction Properties of

Carbon Materials used for Prebaked Anodes in Aluminum Production Plants. *Powder Technology*, 246:650–657, 2013.

[8] Kamran Azari. *Investigation of the Materials and Paste Relationships to Improve Forming Process and Anode Quality*. PhD thesis, Université Laval, 2013.

[9] Kristine Louise Hulse. Rheological Behaviour. In *Anode Manufacture: Raw materials, Formulation and Processing Parameters*, chapter 6, pages 283–334. R&D Carbon Limited, Sierre, Switzerland, 1st edition, 2000.

[10] Roozbeh Mollaabbasi, Thierno Saidou Barry, Seyed Mohammad Taghavi, Donald Ziegler, and Houshang Alamdari. Rheological Characterization of Pitch and Binder Matrix. *ICSOBA*, pages 1–8, 2018.

[11] Roozbeh Mollaabbasi, Lene Jensberg Hansen, Thierno Saidou Barry, Tor Grande, Seyed Mohammad Taghavi, Donald Ziegler, and Houshang Alamdari. Rheological Characterization of Pitch and Binder Matrix with Different Concentrations of Fine Particles. *ICSOBA*, pages 1–8, 2019.

[12] Rafael J Tosta M and Evelyn Mercedes Inzunza. Structural Evaluation of Coke of Petroleum and Coal Tar Pitch for the Elaboration of Anodes in the Industry of the Aluminium. pages 887–892, 2008.

[13] Kristine Louise Hulse. Impact of Raw Materials and Formulation. In *Anode Manufacture: Raw materials, Formulation and Processing Parameters*, chapter 3, pages 77–158. R&D Carbon Limited, Sierre, Switzerland, 1st edition, 2000.

[14] Jean-Pierre Gagné, Marc-André Thibault, Gilles Dafour, Claude Gauthier, Michel Gendron, and Marie-Claude Vaillancourt. Anode Buts Automated Visual Inspection System. *Light Metals*, pages 895–898, 2008.

[15] Werner K Fischer and Raymond C Perruchoud. Interdependence Between Properties of Anode Butts and Quality of Prebaked Anodes. *Light Metals*, pages 33–43, 1991.

[16] Kristine Louise Hulse. Binder Demand. In *Anode Manufacture: Raw materials, Formulation and Processing Parameters*, chapter 4, pages 159–206. R&D Carbon Limited, Sierre, Switzerland, 1st edition, 2000.

[17] Stian Madshus. *Thermal Reactivity and Structure of Carbonized Binder Pitches*. PhD thesis, Norwegian University of Science and Technology (NTNU), 2005.

[18] Jinan Cao, Alan N. Buckley, and Alan Tomsett. Re-Examining the Pitch/coke wetting and penetration test. *JOM*, 54(2):30–33, 2002.

[19] P. Couderc, P. Hyvernat, and J. L. Lemarchand. Correlations between Ability of Pitch to Penetrate Coke and the Physical Characteristics of Prebaked Anodes for the Aluminium Industry. *Fuel*, 65(2):281–287, 1986.

[20] Raymond C. Perruchoud, Markus W. Meier, and Werner Fischer. Worldwide Pitch Quality for Prebaked Anodes. *Light Metals*, pages 509–517, 2003.

[21] J. A. Branscomb. Carbon Electrode Pitches. In A. J. Hoiberg, editor, *Bituminous Materials: Asphalts, Tars and Pitches*, chapter 12, pages 359–384. John Wiley and Sons Inc., 3 edition, 1966.

[22] J. A. Branscomb, V. L. Bullough, and H. A. Morrissey. Relationship of Pitch Properties to Anode Properties. In *Proceedings of the Div. Of Gas and Fuel Chem. National Meeting of the Am. Chem. Soc.*, pages 115–123, New Work, 1960.

[23] T. Ross, K. Krupinski, and M. McClung. Plant Statistical Evaluation of the Effect of Aggregate Composition and Pitch Level on Anode Distortion and Predicted Performance. *Light Metals*, pages 637–643, 1998.

[24] Francisco E Figueiredo, Ciro R Kato, Aluisio S Nascimento, Alberto F Marques, and Paulo Miotto. Finer Fines in Anode Formulation. *Light Metals*, pages 318–321, 2005.

[25] David Belitskus. Standardization of Calcined Coke Bulk Density Test. *Light Metals*, pages 673–689, 1982.

[26] Randall Bowers, Shridas Ningileri, David C Palmlund, Bernie Vitchus, and Frank Cannova. New Analytical Methods to Determine Calcined Coke Porosity , Shape , and Size. *Light Metals*, pages 875–880, 2008.

[27] Turid Vidvei, Trygve Eidet, and Morten Sørlie. Paste Granulometry and Soderberg Anode Properties. *Light Metals*, 2003.

[28] Stein Rørvik, Arne Petter Ratvik, and Trygve Foosnæs. Characterization of Green Anode Materials by Image Analysis. *Light Metals*, pages 553–558, 2006.

[29] Markus W. Meier, Werner K. Fischer, Raymond C. Perruchoud, and Ludwig J. Gauckler. Thermal Shock of Anodes - A Solved Problem? *Light Metals*, pages 700–709, 1994.

[30] Les Edwards, Nigel Baekhouse, Hans Darmstadt, and Marie-Josée Dion. Evolution of Anode Grade Coke Quality. *Light Metals*, pages 1207–1212, 2012.

[31] Kristine Louise Hulse. The Paste Plant. In *Anode Manufacture: Raw materials, Formulation and Processing Parameters*, chapter 2, pages 21–76. R&D Carbon Limited, Sierre, Switzerland, 1st edition, 2000.

[32] David Belitskus. Effects of Mixing Variables and Mold Temperature on Prebaked Anode Quality. *Light Metals*, pages 915–924, 1985.

[33] M. Tkac, T. Foosnaes, and H.A. Øye. Effect of vacuum vibroforming on porosity development during anode baking. *Light Metals*, pages 885–890, 2007.

[34] S. Pérez Pérez, J. Doval-Gandoy, A. Ferro, and F. Silvestre. Quality Improvement for Anode Paste used in Electrolytic Production of Aluminium. *Fourtieth IAS Annual Meeting. Conference Record of the 2005 Industry Applications Conference*, 1:523–528, 2005.

[35] Kristine Louise Hulse. Green Mill Processing Parameters. In *Anode Manufacture: Raw materials, Formulation and Processing Parameters*, chapter 5, pages 207–282. R&D Carbon Limited, Sierre, Switzerland, 1st edition, 2000.

[36] Roozbeh Mollaabbasi. Anode Forming: Rheological Approach. 2019.

[37] Stéphane Thibodeau. *Caractérisation des Propriétés Mécaniques de la Pâte de Carbone à 150C Dans le but D'optimiser la Mise en Forme des Anodes Utilisées dans les Cuves Hall-Héroult*. PhD thesis, Université Laval, 2016.

[38] D. Gates, C. Gallagher, B. Benjamin, N. Fowkes, and J. Ockendon. Modelling and Simulation of a Vibroformer for Carbon Anodes used in Aluminium Production. *Proceedings of the 1992 Mathematics-in-Industry Study Group*, pages 1–16, 1992.

[39] Friedherz Becker and Frank Goede. Ring Pit Furnaces for Baking of high quality Anodes – an Overview. *Aluminium*, (82):9, 2006.

[40] Refratechnik. Primary Aluminium Applications, Concepts for Anode Baking Furnaces. [cited 09.10.2018]. Available from https://www.refra.com/en/Anode-baking-furnaces/, 2018.

[41] H. A. Barnes, J. F. Hutton, and K. Walters. *An Introduction to Rheology*. Elsevier, 1989.

[42] Jonathan J Stickel and Robert L Powell. Fluid Mechanics and Rheology of Dense Suspensions. *Annual Review of Fluid Mechanics*, 37, 2005.

[43] Howard A Barnes. The Yield Stress - a Review or 'Panta Roi' - Everything Flows? *Journal of Non-Newtonian Fluid Mechanics*, 81:133–178, 1999.

[44] Eugene Cook Bingham. *Fluidity and Plasticity*. McGraw-Hill, 1922.

[45] W. H. Herschel and R. Bulkley. Measurement of Consistency as Applied to Rubber-Benzene Solutions. *American Society for Testing Materials*, 26(2):621–633, 1926.

[46] Norman J Wagner and John F Brady. Shear Thickening in Colloidal Dispersions. *Physics Today*, 62(10):27–32, 2009.

[47] H. A. Barnes. Shear-Thickening ("Dilatancy") in Suspensions of Nonaggregating Solid Particles Dispersed in Newtonian Liquids. *Journal of Rheology*, 33:329–366, 1989.

[48] R. L. Hoffman. Observation of a Flow Instability Discontinuous and Dilatant Viscosity Behavior in Concentrated Suspensions. I. Observation of a Flow Instability. *Transactions of the Society of Rheology*, 16(1):155–173, 1972.

[49] Élisabeth Guazzelli and Olivier Pouliquen. Rheology of Dense Granular Suspensions. *Journal of Fluid Mechanics*, 852:1–73, 2018.

[50] John F. Brady and Georges Bossis. The Rheology of Concentrated Suspensions of Spheres in Simple Shear Flow by Numerical Simulation. *Journal of Fluid Mechanics*, 155:105–129, 1985.

[51] John F. Brady and Georges Bossis. Stokesian Dynamics. *Annual Review of Fluid Mechanics*, 20:111–57, 1988.

[52] Jonathan W. Bender and Norman J. Wagner. Optical Measurement of the Contribution of Colloidal Forces to the Rheology of Concentrated Suspensions. *Journal of Colloid and Interface Science*, 172:171–184, 1995.

[53] Jonathan Bender and Norman J. Wagner. Reversible Shear Thickening in Monodisperse and Bidisperse Colloidal Dispersions. *Journal of Rheology*, 40:899–916, 1996.

[54] Brent J. Maranzano and Norman J. Wagner. The Effects of Particle Size on Reversible Shear Thickening of Concentrated Colloidal Dispersions. *The Journal of Chemical Physics*, 114:10514–10527, 2001.

[55] Xiang Cheng, Jonathan H. Mccoy, Jacob N. Israelachvili, and Itai Cohen. Imaging the Microscopic Structure of Shear Thinning and Thickening Colloidal Suspensions. *Science*, 333:1276–1279, 2011.

[56] D. Lootens, P. Hébraud, E. Lécolier, and H. van Damme. Gelation , Shear-Thinning and Shear-Thickening in Cement Slurries. *Oil & Gas Science and Technology*, 59:31–40, 2004.

[57] J. C. van der Werff and C. G. de Kruif. Hard-Sphere Colloidal Dispersions: The Scaling of Rheological Properties with Particle Size, Volume Fraction, and Shear Rate. *Journal of Rheology*, 33:421–454, 1989.

[58] Shirley C. Tsai and Kamel Zammouri. Role of Interparticular Van der Waals Force in Rheology of Concentrated Suspensions. *Journal of Rheology*, 32:737–750, 1988.

[59] Eric Brown and Heinrich M. Jaeger. The Role of Dilation and Confining Stresses in Shear Thickening of Dense Suspensions. *Reports on Progress in Physics*, 77:875–923, 2014.

[60] Albert Einstein. Eine Neue Bestimmung der Moleküldimensionen. *Annalen der Physik*, 19:289–306, 1906.

[61] Albert Einstein. Berichtigung zu meiner Arbeit: "Eine neue Bestimmung der Moleküldimensionen. *Annalen der Physik*, 339:591–592, 1911.

[62] R. Roscoe. The Viscosity of Suspensions of Rigid Spheres. *British Journal of Applied Physics*, 3:267–269, 1952.

[63] H. C. Brinkman. The Viscosity of Concentrated Suspensions and Solutions. *The Journal of Chemical Physics*, 20:571–571, 1952.

[64] Robert Simha. A Treatment of the Viscosity of Concentrated Suspensions. *Journal of Applied Physics*, 23:1020–1024, 1952.

[65] G. K. Batchelor. The Effect of Brownian Motion on the Bulk Stress in a Suspension of Spherical Particles. *Journal of Fluid Mechanics*, 83:97–117, 1977.

[66] Irvin M. Krieger and Thomas J. Dougherty. A Mechanism for Non-Newtonian Flow in Suspensions of Rigid Spheres. *Transactions of the Society of Rheology*, 3:137–152, 1959.

[67] Samuel H. Maron and Percy E. Pierce. Application of Ree-Eyring Generalized Flow Theory to Suspensions of Spherical Particles. *Journal of Colloid Science*, 11:80–95, 1956.

[68] David Leighton and Andreas Acrivos. Viscous Resuspensions. *Chemial Engineering Science*, 41:1377–1384, 1986.

[69] Jeffrey F. Morris and Fabienne Boulay. Curvilinear Flows of Noncolloidal Suspensions: The Role of Normal Stresses. *Journal of Rheology*, 43:1213–1237, 1999.

[70] Isidro E. Zarraga, Davide A. Hill, and David T. Leighton Jr. The Characterization of the Total Stress of Concentrated Suspensions of Noncolloidal Spheres in Newtonian Fluids. *Journal of Rheology*, 44:185–220, 2000.

[71] Birnur K. Aral and Dilhan M. Kalyon. Viscoelastic material functions of noncolloidal suspensions with spherical particles. *Journal of Rheology*, 41(3):599–620, 2002.

[72] D. Chan and R. L. Powell. Rheology of Suspensions of Spherical Particles in a Newtonain and Non-Newtonian Fluid. *Journal of Non-Newtonian Fluid Mechanics*, 15:165–170, 1984.

[73] B. Abdul Haleem and Prabhu R. Nott. Rheology of Particle-Loaded Semi-Dilute Polymer Solutions. *Journal of Rheology*, 53:383–400, 2009.

[74] E. M. Gildebrandt, V. K. Frizorger, E. P. Vershinina, and E. D. Kravtsova. The Viscosity of Pitches and Coke Pitch Compositions. *Metallurgy of Non-Ferrous Metals*, 49:456–458, 2008.

[75] E. M. Gildebrandt, V. K. Frizorger, and E. P. Vershinina. The Effect of the Granulometric Composition and Content of a Coke Charge on the Viscosity of Pitch - Coke Compounds. *Metallurgy of Non-Ferrous Metals*, 50:30–32, 2009.

[76] E. D. Kravtsova, E. M. Gildebrandt, and V. K. Frizorger. Plastic Properties of Pitch - Coke Compositions. *Metallurgy of Non-Ferrous Metals*, 50:114–117, 2009.

[77] E. P. Vershinina, E. M. Gildebrandt, and V. K. Frizorger. Plastic Properties of Homogenized Coke – Pitch Compositions. *Metallurgy of Non-Ferrous Metals*, 52:205–208, 2011.

[78] Thomas G. Mezger. *The Rheology Handbook: for users of Rotational and Oscillatory Rheometers*. Vincentz Network GmbH & Co KG, 2006.

Appendix A

Viscosity of Fluid Models

A.1 Xanthan Solution

Table A.1: Viscosity of Xanthan solution of low concentrations (100, 200, 500, 800 and 1000 ppm) with shear stress from 0 to 100 1/s.

	Viscosity (Pa·s)				
Conc. (ppm)	100	200	300	400	500
Shear rate (1/s)					
0,50	-0,13	-0,054	-0,041	0,074	0,32
0,63	0,15	0,14	0,23	0,34	0,22
0,79	-0,018	-0,033	0,051	0,14	0,20
1,00	0,052	0,070	0,12	0,20	0,16
1,26	-0,019	-0,017	0,038	0,10	0,16
1,58	0,0099	0,0090	0,063	0,12	0,14
1,99	0,0084	0,015	0,055	0,11	0,12
2,51	0,015	0,015	0,057	0,10	0,11
3,15	0,0027	0,0088	0,041	0,079	0,097
3,97	0,0056	0,0090	0,040	0,073	0,085
5,00	0,0041	0,0085	0,035	0,064	0,075
6,29	0,0046	0,0080	0,032	0,057	0,065
7,92	0,0032	0,0064	0,028	0,050	0,057
9,98	0,0040	0,0071	0,026	0,045	0,050
12,56	0,0033	0,0060	0,023	0,039	0,044
15,81	0,0032	0,0057	0,021	0,035	0,038
19,91	0,0028	0,0051	0,018	0,030	0,034

25,06	0,0024	0,0045	0,016	0,026	0,029
31,55	0,0022	0,0042	0,014	0,023	0,025
39,72	0,0021	0,0038	0,013	0,020	0,022
50,00	0,0020	0,0036	0,011	0,018	0,019
62,95	0,0019	0,0034	0,010	0,016	0,017
79,24	0,0018	0,0032	0,0092	0,014	0,015
99,76	0,0018	0,0030	0,0085	0,013	0,013
100,00	0,0018	0,0030	0,0085	0,012	0,013

A.2 Carbopol Gel

Table A.2: Viscosity of Carbopol gel of low concentrations (0.2 % and 0.3 %) with shear stress from 0 to 100 1/s.

	Viscosity (Pa·s)	
Conc. (ppm)	100	200
Shear rate (1/s)		
0,50	-0,091	-0,096
0,63	0,043	0,059
0,79	0,0052	-0,000010
1,00	0,00059	0,0095
1,26	-0,010	-0,011
1,58	0,0065	0,0080
1,99	0,0018	0,0042
2,51	0,0050	0,0078
3,15	-0,0016	0,00094
3,97	0,0017	0,0045
5,00	0,0008	0,0036
6,29	0,0019	0,0047
7,92	0,0016	0,0042
9,98	0,0021	0,0048
12,56	0,0020	0,0045
15,81	0,0020	0,0044
19,91	0,0020	0,0043
25,06	0,0019	0,0041
31,55	0,0019	0,0039
39,72	0,0019	0,0038
50,00	0,0019	0,0038
62,95	0,0019	0,0037
79,24	0,0019	0,0036
99,76	0,0019	0,0036
100,00	0,0019	0,0036